AD-A186 858 VARIABLE BAND GAP MATERIALS FOR THERMOPHOTOVOLTAIC GENERATORS(U) BEIJING UNIV (CHINA) IRON AND STEEL COLL* L D WOOLF ET AL AUG 87 GA-A18953 AFOSR-TR-87-1517 1/1

UNCLASSIFIED F49620-86-C-0043 F/G 10/2 NL

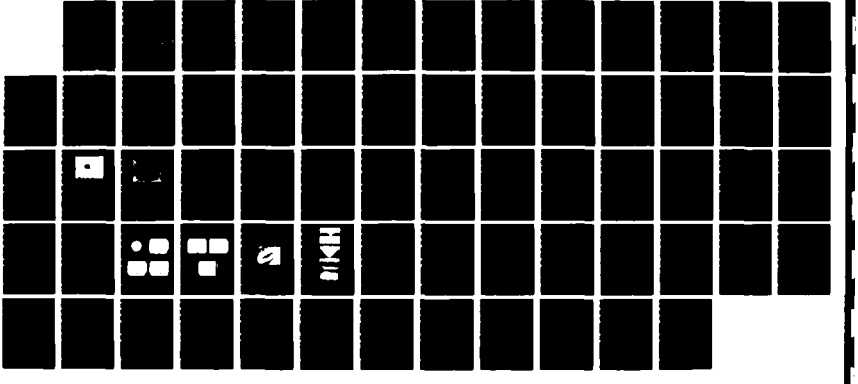

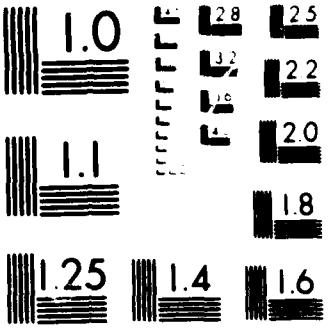

(2)

GA Technologies

AFOSR-TR- 87-1537 GA-A18953

VARIABLE BAND GAP MATERIALS FOR THERMOPHOTOVOLTAIC GENERATORS

FINAL TECHNICAL REPORT
FOR THE PERIOD
APRIL 1, 1986 TO AUGUST 31, 1987

by
L. D. WOOLF, D. M. DUGGAN
and J. N. SMITH, JR.

Prepared under
Contract F49620-86-C-0043
for the Air Force Office of Scientific Research

AUGUST 1987

SECURITY CLASSIFICATION OF THIS PAGE

AD-A186 858

REPORT DOCUMENTATION PAGE

Form Approved
OMB No. 0704-0188

1a. REPORT SECURITY CLASSIFICATION Unclassified	1b. RESTRICTIVE MARKINGS None
2a. SECURITY CLASSIFICATION AUTHORITY	3. DISTRIBUTION / AVAILABILITY OF REPORT Unlimited
2b. DECLASSIFICATION / DOWNGRADING SCHEDULE	
4. PERFORMING ORGANIZATION REPORT NUMBER(S) GA-A18953	5. MONITORING ORGANIZATION REPORT NUMBER(S) AFOSR-TR- 87-1537
6a. NAME OF PERFORMING ORGANIZATION GA Technologies Inc.	6b. OFFICE SYMBOL (If applicable) GA
6c. ADDRESS (City, State, and ZIP Code) San Diego, CA 92138	7a. NAME OF MONITORING ORGANIZATION Air Force Office of Scientific Research
	7b. ADDRESS (City, State, and ZIP Code) Bolling AFB, DC 20332-6448
8a. NAME OF FUNDING / SPONSORING ORGANIZATION Air Force Office of Scientific Research	8b. OFFICE SYMBOL (If applicable) NP
8c. ADDRESS (City, State, and ZIP Code) Bolling AFB, DC 20332-6448	9. PROCUREMENT INSTRUMENT IDENTIFICATION NUMBER F 49620-86-C-0043
	10. SOURCE OF FUNDING NUMBERS PROGRAM ELEMENT NO. 61102F; PROJECT NO. 2301; TASK NO. A7; WORK UNIT ACCESSION NO.

11. TITLE (Include Security Classification)
Variable Band Gap Materials for Thermophotovoltaic Generators

12. PERSONAL AUTHOR(S)
Woolf, Lawrence D.; Duggan, Dennis M.; Smith, Joe N., Jr.

13a. TYPE OF REPORT	13b. TIME COVERED	14. DATE OF REPORT (Year, Month, Day)	15. PAGE COUNT
Final	FROM 4/1/86 TO 8/31/87	August 1987	59

16. SUPPLEMENTARY NOTATION

17. COSATI CODES		
FIELD	GROUP	SUB-GROUP

18. SUBJECT TERMS (Continue on reverse if necessary and identify by block number)
Thermophotovoltaic Energy Conversion; GaAs Solar Cells; Photochemical etching; GaAs; Free Carrier Absorption; Infra-Red Reflectivity

19. ABSTRACT (Continue on reverse if necessary and identify by block number)
The objective of this research program was to design and develop direct band gap solar cells which would have high below band gap energy (infra-red (IR)) reflectivity for use in high efficiency thermophotovoltaic (TPV) energy conversion systems. Two types of customized GaAs cells were grown on intrinsic or semi-insulating GaAs substrates with either p-type GaAs or $Al_{0.9}Ga_{0.1}As$ stop-etch layers. Holes were drilled through the substrate using a laser photochemical and/or chemical etch technique. Cells with high IR reflectivity and low series resistance were fabricated by drilling a hole which stopped at the contact layer of the cell with the $Al_{0.9}Ga_{0.1}As$ stop-etch layer and then depositing gold in the hole and on the back surface. Measurements of these customized cells indicate that IR reflectivities in excess of 90%, corresponding to TPV efficiencies in excess of 35%, are feasible.

20. DISTRIBUTION / AVAILABILITY OF ABSTRACT ☒ UNCLASSIFIED/UNLIMITED ☐ SAME AS RPT ☐ DTIC USERS	21. ABSTRACT SECURITY CLASSIFICATION Unclassified
22a. NAME OF RESPONSIBLE INDIVIDUAL BRUCE C. SMITH	22b. TELEPHONE (Include Area Code) (202) 767-4907
	22c. OFFICE SYMBOL NP

DD Form 1473, JUN 86 Previous editions are obsolete SECURITY CLASSIFICATION OF THIS PAGE

GA Technologies

GA-A18953

VARIABLE BAND GAP MATERIALS FOR THERMOPHOTOVOLTAIC GENERATORS

FINAL TECHNICAL REPORT
FOR THE PERIOD
APRIL 1, 1986 TO AUGUST 31, 1987

by
L. D. WOOLF, D. M. DUGGAN
and J. N. SMITH, JR.

Prepared under
Contract F49620-86-C-0043
for the Air Force Office of Scientific Research

GA PROJECT 3822
AUGUST 1987

Contents

FIGURES

TABLES

1. INTRODUCTION AND RESEARCH OBJECTIVES

Thermophotovoltaic (TPV) energy converters use a heat source to raise the temperature of an emitter material so that it emits photons. When absorbed in a photovoltaic cell, those photons with energy above the band gap cause electron-hole pairs to be created and an electric current to flow. The below band gap energy photons are reflected by the cell back to the emitter, conserving that portion of the energy spectrum. The heat source for this process can be a nuclear reactor, a radioactive isotope generator, concentrated solar energy, or a fossil-fuel burner.

To optimize the efficiency of TPV cells, the thermal emitter should operate at a temperature such that the maximum number of photons emitted have an energy closely matched to the band gap energy of the cell photovoltaic material. For typical cell temperatures of 300 to 600°K and emitter temperatures of 1500 to 2300°K, the maximum conversion efficiency occurs for cells with band gaps in the range of ~0.7 to 1.4 eV [1,2]. For a given cell and emitter temperature and weighted parasitic absorption there is an optimum band gap which maximizes the TPV efficiency. The solid solution alloys of InAs-GaAs are quite attractive in that the band gap is direct in these materials and can be varied from 0.35 to 1.4 eV by changing the relative proportion of InAs to GaAs. Significant improvements in the efficiency of TPV energy conversion can be achieved if parasitic photon absorption is minimized so that the

below-band-gap photons are not absorbed in the cell but are reflected back to the thermal emitter to help keep it hot.

TPV cell material for space power applications must be able to operate at a relatively high temperature in order to minimize the mass of the radiator used to transfer waste heat. Lower radiator mass leads to lower specific mass (kg/kW), a major goal in space power applications.

In 1982, GA Technologies Inc. (GA) completed a study for NASA-Lewis Laboratories [3] which indicated that TPV energy conversion has great potential for space power applications. For a 100 kW space nuclear power system, this study indicated that the specific mass for a TPV-based system was 7 to 15 kg/kW. By comparison, the specific mass for comparable thermionic- and thermoelectric-based nuclear space power systems is ~30 kg/kW.

In 1985, a subsequent study [1] performed for the Air Force Office of Scientific Research focused on a theoretical and experimental investigation of variable band gap cells in TPV. In particular, dark and illuminated current versus voltage characteristics were obtained for a number of InGaAs, GaAs and Si concentrator cells at cell temperatures varying from 300 to 550°K. Based on these data, the temperature dependence of the TPV efficiency for each of these cells was inferred for a fixed value of the parasitic absorption of the below band gap energy photons. For a given weighted parasitic absorption of 5%, the InGaAs cells were found to have significantly higher TPV efficiencies than the GaAs or Si cells. TPV efficiencies approaching 40% at 300°K and 26% at 500°K appeared feasible for the InGaAs cells. Based on these data, it was calculated that the specific mass of a space based nuclear-TPV energy conversion system would be 10 kg/kW if InGaAs cells with 5% weighted parasitic absorption were

used. In addition, a theoretical model was developed for determining the optimum efficiency of single and multiple band gap cells in TPV energy conversion.

The objective of the current research program was to design and develop cells based on GaAs substrates, such as InGaAs cells, specifically for TPV applications. These cells would exhibit low parasitic absorption of below band gap energy photons, a requirement for high TPV efficiencies, as discussed above. Two designs were considered for the low parasitic absorption cell development. The objective of both designs was to minimize the primary source of the parasitic absorption which was due to the heavily doped single crystal GaAs substrate upon which the InGaAs and GaAs active regions (*i.e.*, $p-n$ junction, window and contact layers) are grown.

In the thin cell approach, previously examined by others [4,5], the GaAs cell is bonded to a superstrate, and then the substrate is etched down to the active regions of the cell. Typically an etchant is used which etches GaAs but not AlGaAs, which is the layer adjacent to the substrate, in order to perform this operation. For this program, it was decided that the thin cell approach would not be followed for a variety of reasons. First, this type of cell had previously been developed and similar concepts are currently being examined for use in stacked multiple band gap cell programs. Since the objective of this AFOSR-funded research was to further basic research and not to further development of currently existing methods, an entirely new approach for a low parasitic absorption cell was chosen, as discussed below. Another disadvantage of the thin cell is that when the substrate is etched off, all that remains is a $\sim$5 micron thick cell (the active regions) bonded to the superstrate. The thinness of this resultant cell makes fabrication of electrical contacts to both the top and bottom of the cell difficult. In addition, the adhesive used to bond the superstrate to the cell limits the high temperature operating limit of the cell to the vicinity of the melting point of the

adhesive. Finally, in making the electrical contact to the back of the (etched) cell, the metal contact material is deposited and then alloyed to produce a low resistance ohmic contact. While required for a low resistance contact, this alloying step will tend to reduce the reflectivity of the back surface mirror, which is also the electrical contact, since the alloying results in some diffusion at the metal/semiconductor interface.

The shorted substrated cell design approach was chosen to be the focus of the research effort under this program. As shown in Fig. 12, the design of this cell is quite unlike any other type of solar cell currently under development. Thus, the basic research needed to fabricate and measure the properties of this cell responded to the mission of AFOSR. In this design, the active region of the cell is grown on an intrinsic or nearly intrinsic (lightly doped) GaAs substrate. Previous calculations [1] had indicated that the weighted parasitic absorption of such a cell would be quite low, less than or on the order of 5%. The intrinsic substrate would not be expected to contribute to free carrier absorption in the below band gap energy regime, since the parasitic absorption is proportional to the free carrier density. In order to reduce the series resistance of the cell, holes would be drilled through the GaAs substrate to a contact layer and filled with a metallic conductor. Thus, since the cross-sectional area of the substrate would predominantly consist of intrinsic GaAs, free carrier absorption due to the substrate would be expected to be minimal. In addition, the series resistance of the cell would also be low, due to the highly conductive metallic shorting tubes which would transport the current from the heavily doped GaAs contact layer to the bottom of the substrate. There are a number of advantages to this cell design. First, the cell is structurally identical to commercially available cells in that the top and bottom contacts are in the same positions and that the thickness is the same as standard cells. Secondly, the alloying step required to form a low resistance ohmic contact between the GaAs contact layer and the top of the metal tube can be

performed prior to the mirror deposition. Thus, the cell may have a low resistance contact and a highly reflective back surface mirror.

While InGaAs cells are likely to be preferred for TPV applications, as discussed above, GaAs substrates and cells were the primary materials investigated in this program. This arose for two reasons. First, InGaAs cells are grown on GaAs single crystal substrates so that an investigation of the properties and characteristics of commercially available GaAs substrates was appropriate. Second, InGaAs cells are more difficult to grow than GaAs cells since the InGaAs cells involve a third component and also require graded layers between the GaAs substrate and the $p-n$ junction to accommodate the lattice mismatch between the GaAs and InGaAs. Thus, the fabrication of customized GaAs cells was chosen over that of InGaAs for reasons of price and delivery time.

To reiterate, the primary objective of this research effort was to examine methods of fabrications of GaAs shorted substrate cells and to measure both the below band gap energy absorptance, transmittance, and reflectance (for those samples with back surface reflectors) as well as the electrical properties, in particular, the series resistance of the completed cell. Based on these data, the performance of a TPV system using these cells was to be evaluated.

2. THEORETICAL ANALYSES

Before any thermophotovoltaic (TPV) cells were made, the feasibility of the shorted substrate design was established by calculations of the series resistance and the infra-red reflectivity. In addition, a brief discussion of photo-assisted etching of doped semiconductors is included for completeness.

2.1. SUBSTRATE SERIES RESISTANCE

The substrate series resistance considered in this section consists of two components. The first component is comprised of n shorting tubes in parallel *i.e.*, the metal-filled holes fabricated in the insulating substrate. The second component is represented by the restricted current flow in the heavily doped layer between the $p-n$ junction and the ohmic contacts to the ends of the shorting tubes. Calculation of the resistance of the shorting tubes is straightforward but approximations must be made in the case of the intermediate layer. Since the absorption of the cell increases as the series resistance decreases by virtue of increasing the diameter and/or the number of shorting posts, the series resistance of the substrate will remain an important consideration and must be estimated.

To estimate the resistance of the doped intermediate layer, the shorting posts will be taken for simplicity to be rectangular with width W and separated from the $p-n$ junction by an intermediate layer of thickness D as shown in Fig. 1. The current

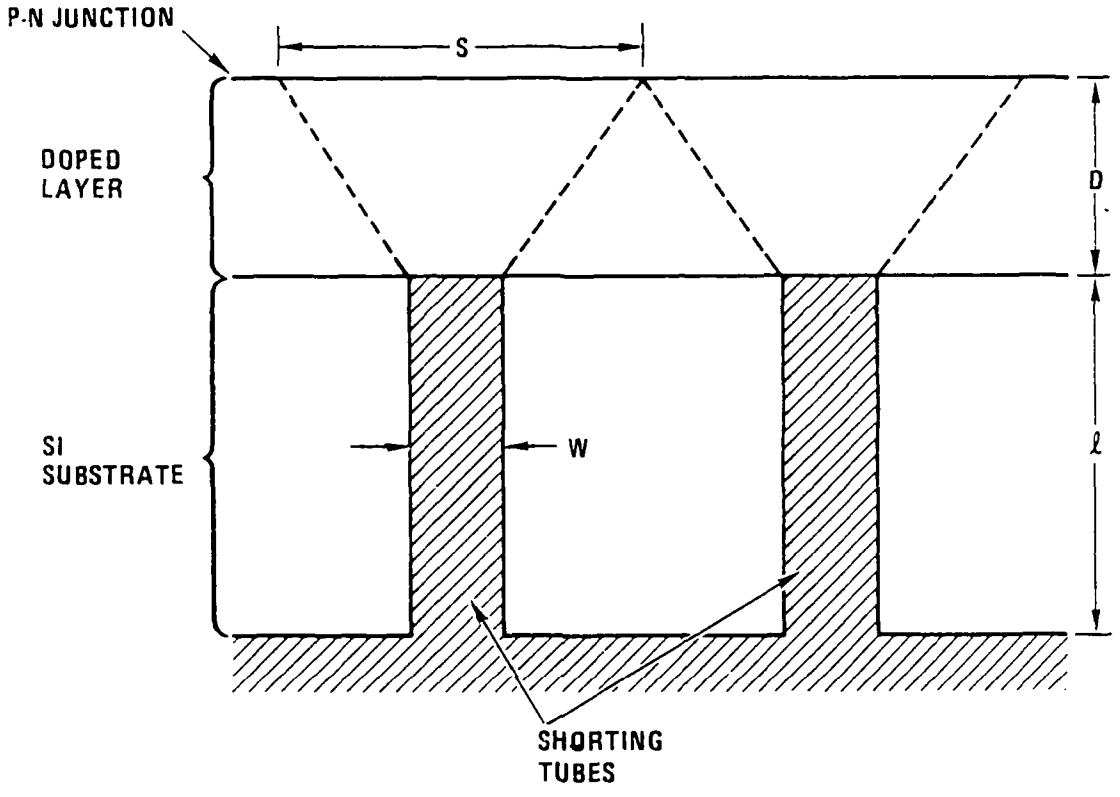

Fig. 1. Structure used to approximate shorted substrate cell for calculation of equivalent series resistance.

channels in the intermediate layer will be approximated by a truncated pyramidal volume with a base dimension S (equal to the post spacing) located at the $p-n$ junction and terminating on the tops of the posts. In 3-dimensions, the resistance of one such channel can be shown to be $R_1 = \rho_{p+} D (WS)^{-1}$, where ρ_{p+} is the resistivity of the doped region. If there are n shorting posts, the parallel resistance of the intermediate layer becomes

$$R_{p+} = \frac{R_1}{n} = \frac{\rho_{p+} SD}{W} \left(\frac{1}{nS^2} \right) = \frac{\rho_{p+} SD}{W A_c} \quad , \tag{1}$$

where $A_c = nS^2$ is the total area of the cell. The parallel resistance of n shorting rods is given by $R_R = \rho_R \, \ell \, A_C^{-1} \, S^2 \, W^{-2}$ where ρ_R is the resistivity of a rod of length ℓ. Then the series resistance of the two substrate components is

$$R_S = \frac{1}{A_c} \left[\rho_{p+} D + \rho_R \ell \left(\frac{S}{W} \right) \right] \frac{S}{W} \quad . \tag{2}$$

Since SW^{-1} cannot be decreased indefinitely, due to increasing cell absorption, a compromise from the resistance standpoint could be taken as the value of SW^{-1} that causes the rod resistance and the doped region resistance to be equal, *i.e.*, equating the two bracketed terms of Eq. (2). Using the values $\rho_R = 1.6 \times 10^{-6}$ Ω-cm, $\rho_{p+} = 1.5 \times 10^{-3}$ Ω-cm, $D = 2 \times 10^{-4}$ cm and $\ell = 3.8 \times 10^{-2}$ cm results in $SW^{-1} = 5$. For $A_c = 0.4$ cm^2, this gives a series resistance $R_s \simeq 8 \times 10^{-6} \Omega$ with 25 equally spaced rods of diameter $W = 2.5 \times 10^{-2}$ cm (0.010″). For comparison, the cell resistance with a single 0.010″ rod would be $\sim 10^{-4} \Omega$. Such cell resistances would lead to negligible power losses for cells operated under high illumination.

2.2. TRANSMISSION AND REFLECTION BY A DIELECTRIC SLAB

As illustrated in Fig. 2, the transmission coefficient, which is simply the ratio of the transmitted to incident light intensity, of a dielectric slab for normal incidence is a sum of terms. The zeroth term is due to rays that pass through once with no reflections, while the nth is due to rays that are reflected off the back and then the front surfaces n times:

$$T = (1 - R_1)^2 x + (1 - R_1)^2 x^3 R_1^2 + \cdots \tag{3}$$

where R_1 is the reflection coefficient for the dielectric-air interface and x is given by

$$x = \exp(-\alpha t) \quad , \tag{4}$$

where α is the absorption coefficient and t the thickness of the slab. The series [Eq. (3)] is easily written by noting that: each ray must pass through the slab at least once and be transmitted through the front and back surfaces once, so that each term includes the factor $(1 - R)^2 x$; each additional double pass through the slab is accounted for by a factor of x^2 and a factor of R_1^2 for the back and front surface reflections. Hence

$$T = (1 - R_1)^2 x \sum_{n=0}^{\infty} (R_1 x)^{2n} \quad . \tag{5}$$

Summing by elementary methods yields

$$T = (1 - R_1)^2 x / [1 - (R_1 x)^2] \quad . \tag{6}$$

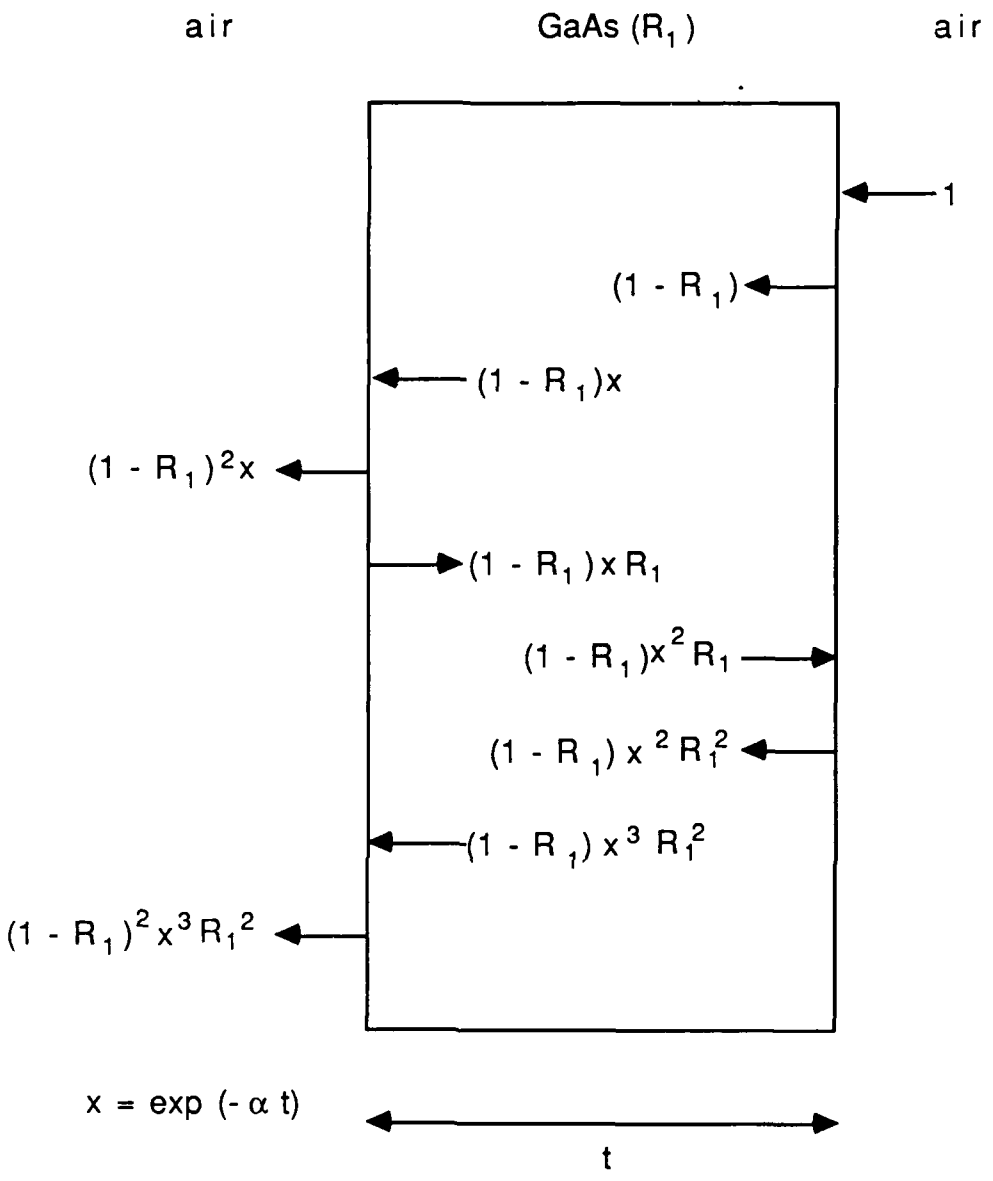

Fig. 2. Transmission through a GaAs slab.

The case of reflection from a dielectric slab with a back surface reflector, illustrated in Fig. 3 is only slightly more complicated. By much the same reasoning that led to Eq. (5), the total reflection coefficient is given by

$$R = R_1 + (1 - R_1)^2 \sum_{n=0}^{\infty} (x^2 R_2)^n = R_1 + (1 - R_1)^2/(1 - x^2 R_2) \quad . \tag{7}$$

2.3. PHOTO-ASSISTED ETCHING OF DOPED III-V SEMICONDUCTORS

The basic mechanism [6] of photodecomposition of an n-type III-V semiconductor is shown in Fig. 4. At the interface between the semiconductor and an oxidizing solution, surface states pin the Fermi level and the bands bend upward as at a semiconductor-metal surface. The region in which the bands are bent is depleted of free carriers. A photon whose energy exceeds the bandgap will create an electron-hole pair. The electric field due to the band bending separates the pair and holes accumulate at the surface. For GaAs, the chemical reaction at the interface can be written as:

$$\mathrm{GaAs} + 6\mathrm{h}^+ \rightarrow \mathrm{Ga}^{+3} + \mathrm{As}^{+3} \quad . \tag{8}$$

A hole, of course, is the absence of an electron in the valence band, which is formed from the bonding orbitals; in other words, it is a broken bond. Three holes can break all the bonds to a Ga or an As atom on the surface so that it can go into solution as an oxide. The ion exchange with the solution may be mediated by the surface states. The Ga^{+3} ion can only dissolve when the solution pH < 3.5 (base)

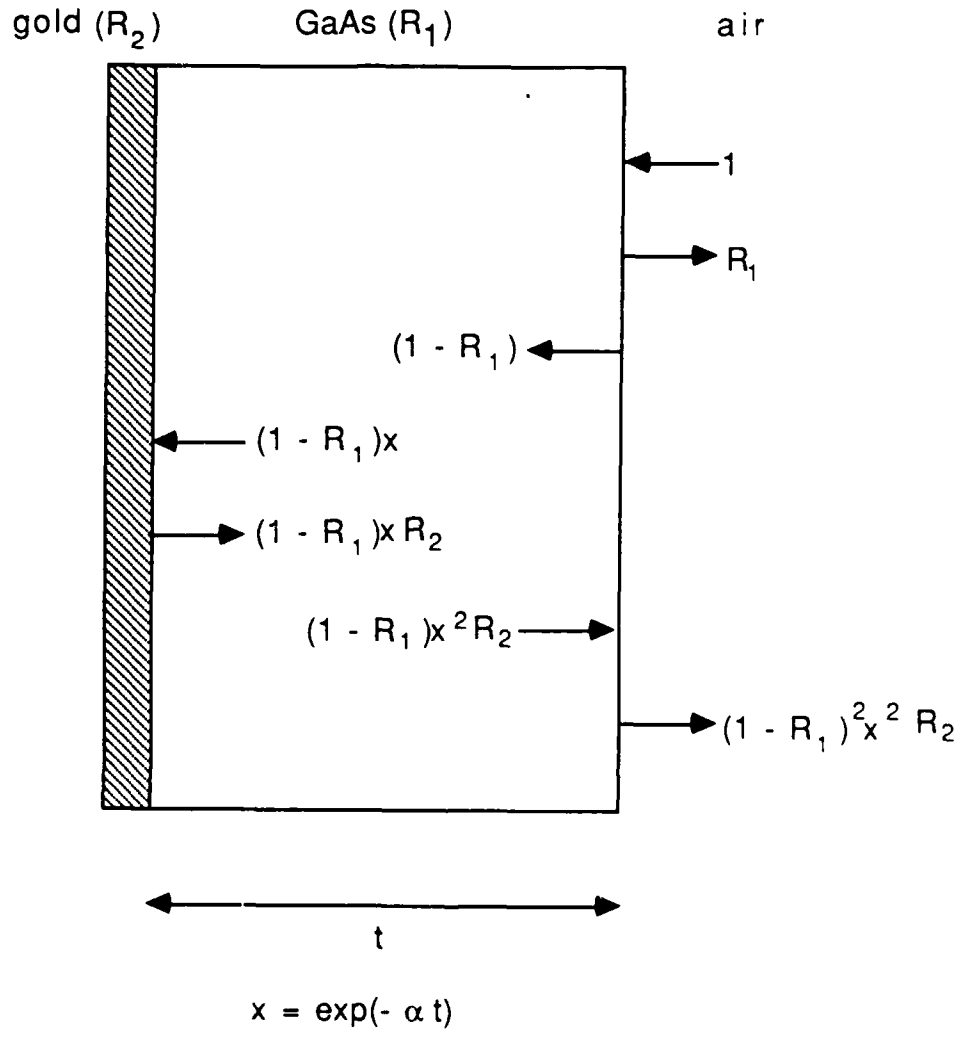

Fig. 3. Reflection from a gold-coated GaAs slab.

or pH > 9 [7]. Since the bands bend in the opposite direction at the surface of p-type GaAs, holes are swept away and etching is actually retarded by the light. The reductive decomposition of p-type GaAs

$$\mathrm{GaAs} + 3\mathrm{e}- \rightarrow \mathrm{Ga} + \mathrm{As}^{-3} \quad , \tag{9}$$

is analogous to Eq. (8) but the Ga atoms remain on the surface and stabilize it [8]. In fact, buildup of any insoluble reaction products on the surface can stop the reaction [7].

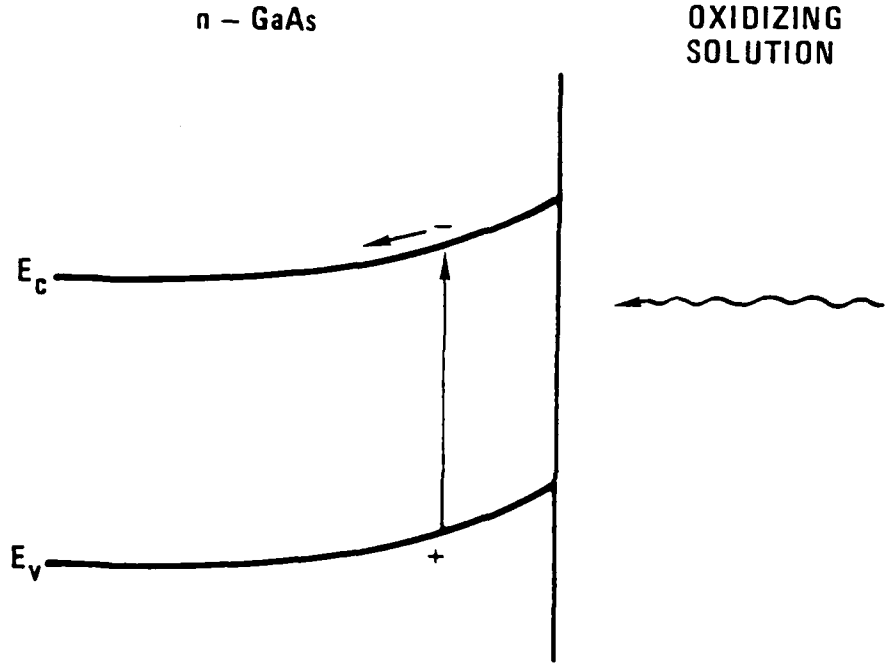

Fig. 4. Band diagram for GaAs/etching solution interface.

3. EXPERIMENTAL TECHNIQUES

3.1. IR TRANSMISSION AND REFLECTION

A Perkin-Elmer 735B Spectrophotometer was used for both the reflection and transmission measurements. A Harrick VMA/RMA accessory was used to mount samples for reflection measurements. Special holders oriented the sample perpendicular to the beam and masked off all of the area outside the sample. Since the Perkin-Elmer 735B is a double beam spectrometer which measures the power transmitted through or reflected from the sample relative to a reference beam, the measured transmission coefficient for the samples was divided by that measured for the holder with no sample and the measured reflection coefficient for light incident on the front side of a TPV cell with a back surface reflector was divided by that measured for light incident on the back side.

3.2. PHOTOETCHING

As shown in Fig. 5, the GaAs wafers and TPV cells were glued to a small Cu slab before photoetching. The copper slab was placed in the center of the bottom half of a simple clamp made from perforated aluminum sheet and a small neoprene O-ring was set on top of the GaAs. Then a low polyethylene beaker with a small hole drilled in the center was set on the O-ring. The holes in the beaker and the O-ring were aligned by a round wooden stick inserted in the beaker hole. The top half of

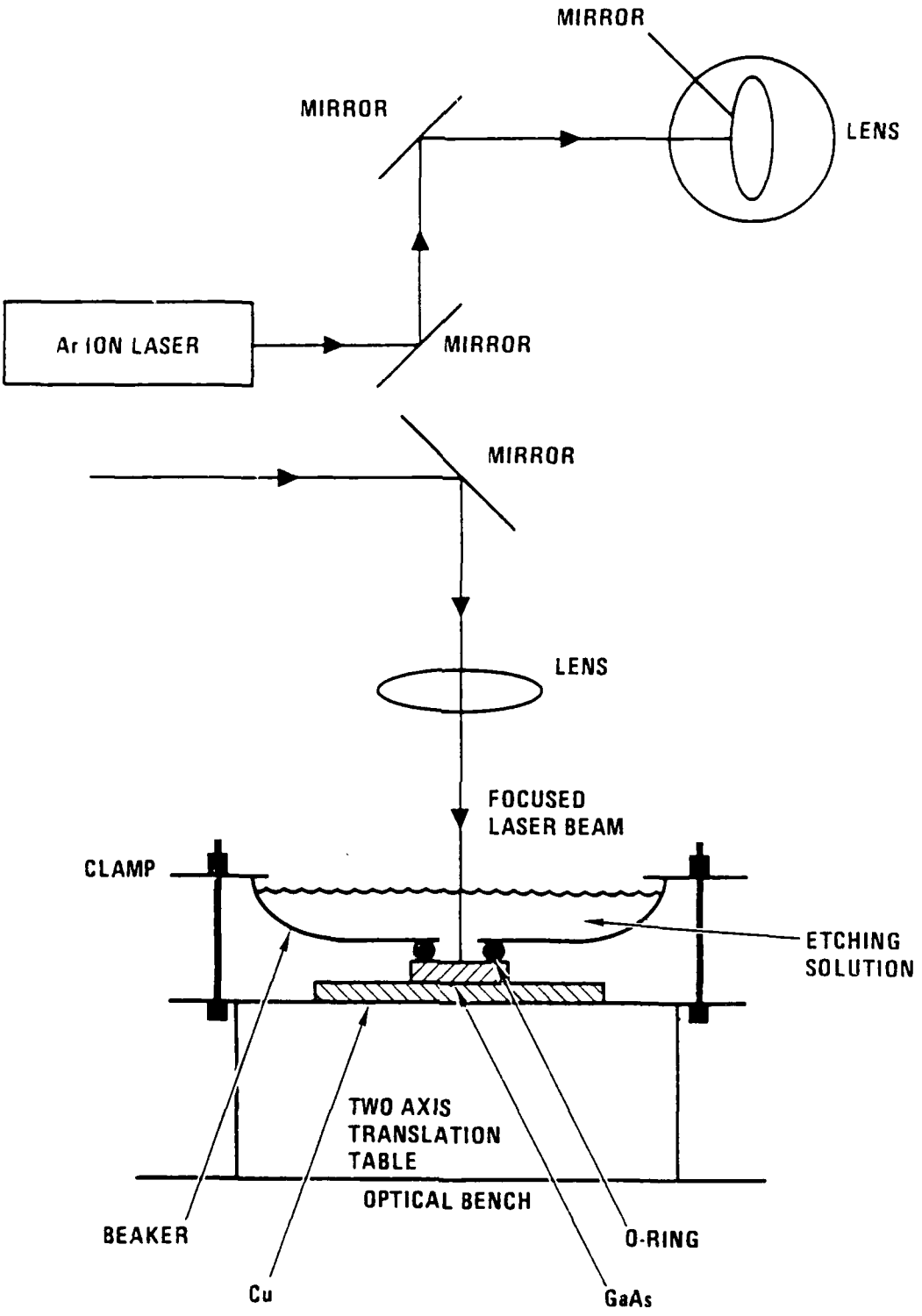

Fig. 5. Schematic of laser photochemical etch experiment.

the clamp, made from the same perforated aluminum sheet by cutting a hole with a radius slightly smaller than the beaker's, was put on top of the beaker and bolted to the bottom half. Thus only the small area of the GaAs inside the O-ring was exposed to the etchant and damage from dark etching was minimized. (Masking off all but a small area of the GaAs by painting it with micromask would have protected it from dark etching just as well, but because the solutions did not wet the micromask, any bubbles formed during photoetching would stick to it.) The solutions containing peroxide always evolved many bubbles and thermal currents caused by the laser beam heating the solution would draw them into the beam where they would scatter the light.) Once the clamp was assembled, it was bolted to a two axis translation table, which was in turn bolted to the optical table under a focusing lens. A Bausch and Lomb Stereozoom microscope with crosshairs mounted on the optical table was used to aim the laser beam and observe the photoetching. A Zeiss microscope with a three axis translation table was used to measure the depth of the holes below the unetched surface and to take photographs at various depths.

3.3. DARK ETCHING

The solutions for dark etching the TPV cells with (AlGa)As stop etch layers were ultrasonically agitated with the arrangement shown in Fig. 6. The cell was placed in the bottom of a beaker of a solution which was in turn partially immersed in water in an ultrasonic cleaner. For the first etch in $57H_2O_2$:$3NH_4OH$:$140H_2O$, which attacks GaAs, all of the cell except for a small area around the photoetched hole was masked off with commercial micromask. Because this solution, like all those containing peroxide, evolves bubbles copiously, the cell was tied to a glass microscope slide with teflon tape and the tape was in turn glued to the slide with micromask so that the cell would not float in the solution. The second etch in the buffered oxide etch

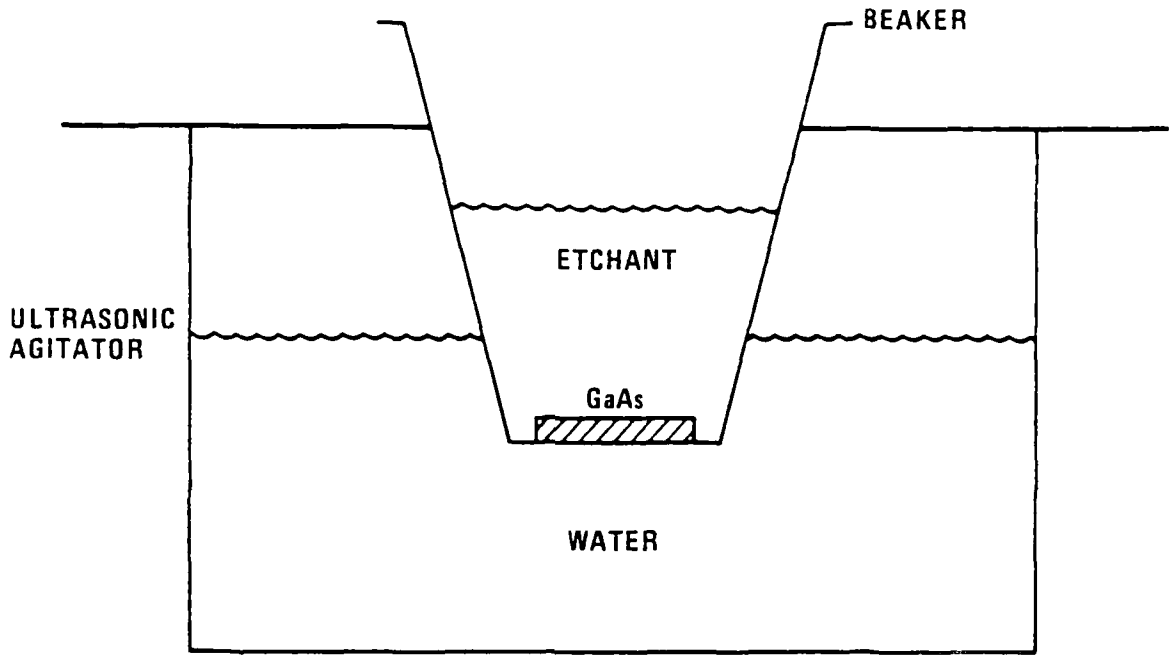

Fig. 6. Diagram of dark etch experiment.

1HF:4NH_4F:7H_2O does not evolve bubbles, so the cell was placed in the bottom of a teflon beaker containing the solution. Since the second etch attacked only AlGaAs, only the sides of the cell were masked off.

4. HOLE DRILLING STUDIES WITH UNIFORMLY DOPED WAFERS

Prior to etching fully fabricated GaAs cells, a number of etching studies were undertaken using intrinsic, *p*-type and *n*-type GaAs single crystal substrates.

4.1. JET THINNING

A South Bay Technology Model 550 jet thinning instrument, normally used for thinning of TEM specimens, was employed in the first attempts at hole drilling. Both an electrolytic etch and a wet chemical etch were tried. In the former case the electrolyte used was $HClO_4$: $4CH_3COOH$, passing $\sim$ 140 ma at 20 V. *p*-doped GaAs was observed to etch very rapidly but semi-insulating (SI) GaAs was not etched at all due to its large resistivity.

The wet chemical etch employed was a solution of H_3PO_4:H_2O_2:$3CH_3OH$. An SI wafer was masked with commercial micromask prior to etching. The etch rate for SI GaAs was very low and there was extensive undercutting of the mask. Further attempts with the jet-thinner were not made since electrolytic schemes were not applicable to the SI material and the wet chemical schemes appeared to be uncontrollable.

4.2. LASER ASSISTED CHEMICAL ETCH

An Ar^+ laser was used at power levels between 0.5 and 2 watts (equal intensities at 5140 and 4880$\mathring{A}$). Appropriate optics were used to produce a beam spot of $\sim$0.010″

diameter or less at the wafer surface. The etch solution used was 32 mℓ H_2O, 8 mℓ of 30% H_2O_2 and 2.5 mℓ H_2SO_4 (or $100H_2O$:$6.4H_2O_2$:$6.4H_2SO_4$). Wafers of *p*-doped, *n*-doped and SI GaAs were studied. The etch features were examined using SEM and optical microscopy and surface profilometry.

The etch rate of the three materials as a function of laser power is indicated in Fig. 7. For these conditions, a laser power of 2 watts corresponds to a power density of approximately 6 kW/cm^2. For the purpose of this program, the region of interest is below a laser power density of about 3 kW/cm^2 (1 watt in Fig. 7). In this region SI GaAs is seen to etch at a rate of about $\leq$10 μm per minute while *p*-doped GaAs has an apparent *negative* etch rate of about $\leq$1 μm per minute. This "negative" etch rate is simply a way of specifying that the etch feature is not a hole in the wafer, but rather a mesa-like structure raised above the surrounding surface. The distinction between these etch features is shown in the comparison of Figs. 8(a,b) with Figs. 9(a,b). Figure 8 contains an SEM photo and profilometer trace of a ~300 μm diameter hole in SI GaAs etched with a laser power of 0.5 watts. Figure 9 shows the same observations of a 15-20 μm high, 250 μm diameter mesa on *p*-doped GaAs produced with a laser power of ~0.52 watts.

From the information in Fig. 9, the origin of the mesa structure is ambiguous: it could have been produced by a buildup of material in the region of illumination or by a recession (dark etch) of the surrounding region. To resolve this question, another *p*-doped wafer was partially covered with micro-mask and "etched" at an unmasked region nearby. Then the micro-mask was removed and a profilometer trace was made that covered both the masked region and the resultant mesa and the result is shown in Fig. 10. After allowing for the curvature of the wafer it is seen that the mesa top coincides very nearly with that portion of the wafer that was masked during the etch,

i.e., the mesa results from the dark etch recession of the area surrounding the point of laser-illumination. To a first approximation, the laser prevents etching in *p*-type GaAs. A similar result was reported in 1972 by Kuhn-Kuhnenfeld [9,11].

While the samples shown in Figs. 8 and 9 were in the SEM, energy-dispersive x-ray analysis (EDAX) was performed. For both the mesa top and the surrounding region of Fig. 9 and the surrounding region of Fig. 8, the Ga:As ratio was very nearly 1:1, however in the hole of Fig. 8, this ratio was 2.7:1, *i.e.*, Ga-rich. Thus, the dark etch removes Ga and As in equal quantities, while the laser assisted etch removes As at an enhanced rate (in SI GaAs).

Without discussion of the possible detailed etch mechanisms occurring in SI and *p*-doped GaAs, the results discussed above suggested a method for "drilling" a hole several hundred μm deep in the SI GaAs substrate of a TPV cell with a depth accuracy on the order of 1 μm or less by using a *p*-doped GaAs stop-etch layer. To test the scheme, several cells were produced to GA Technologies specifications by Varian Associates. The results are reported in the next section.

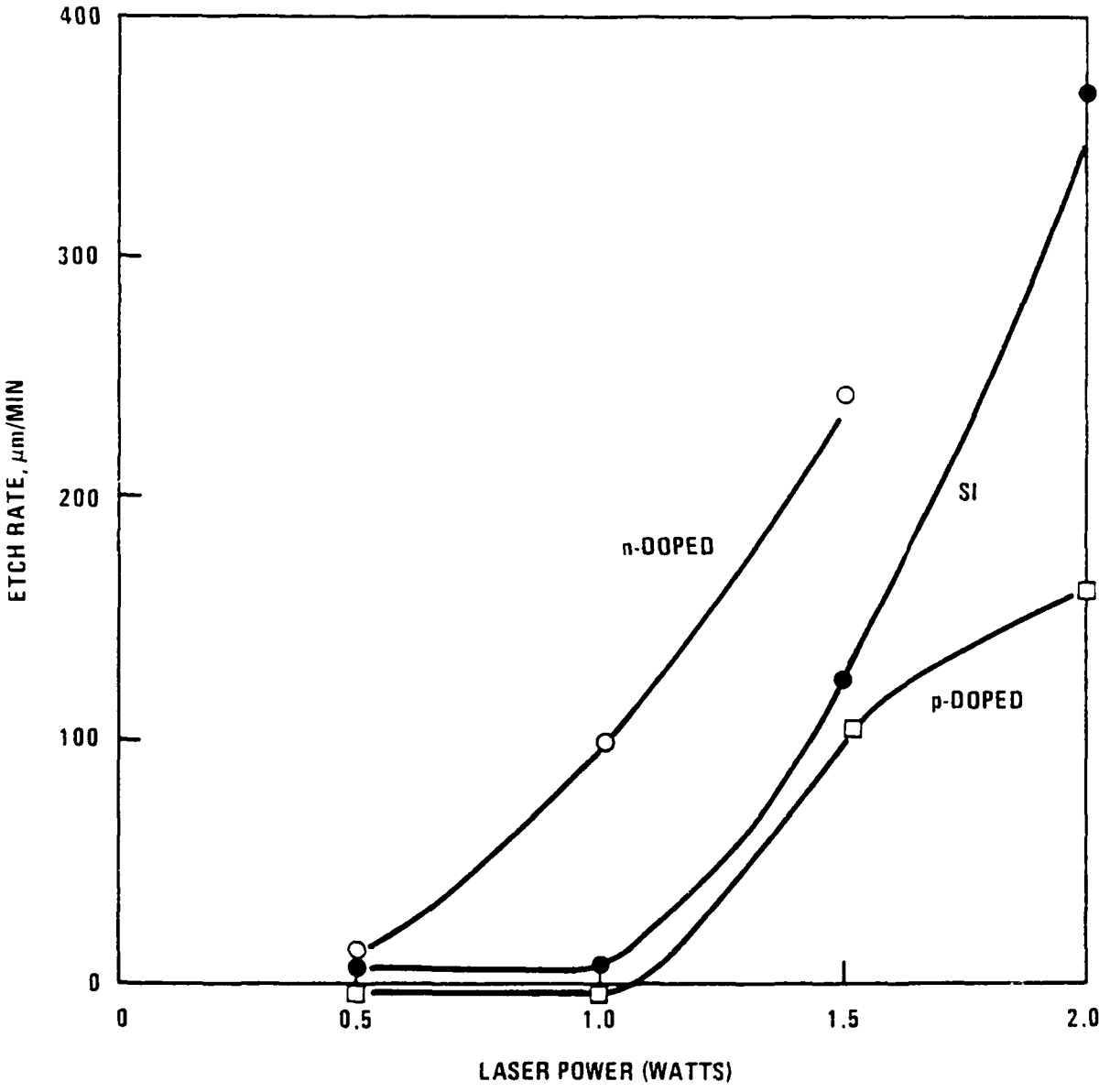

Fig. 7. Etch rate versus laser power for n-type, p-type and SI-GaAs.

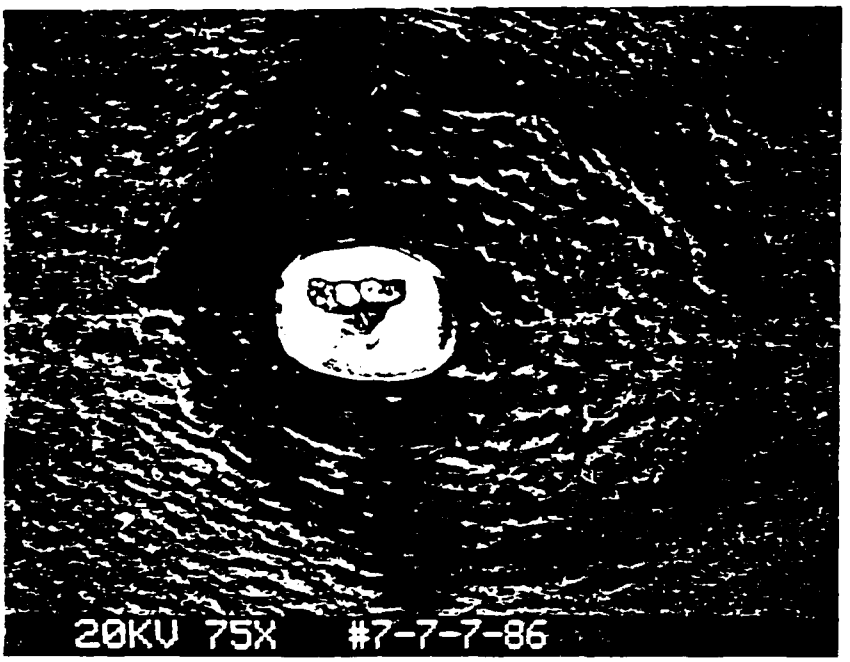

(a)

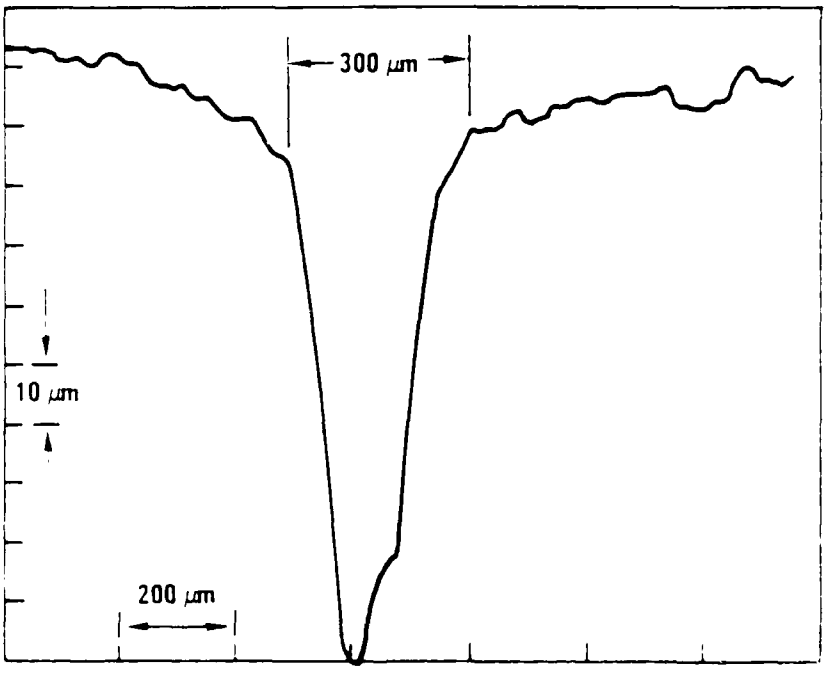

(b)

Fig. 8. (a) SEM photomicrograph and (b) profilometer trace of a laser photochemical produced mesa in SI-GaAs.

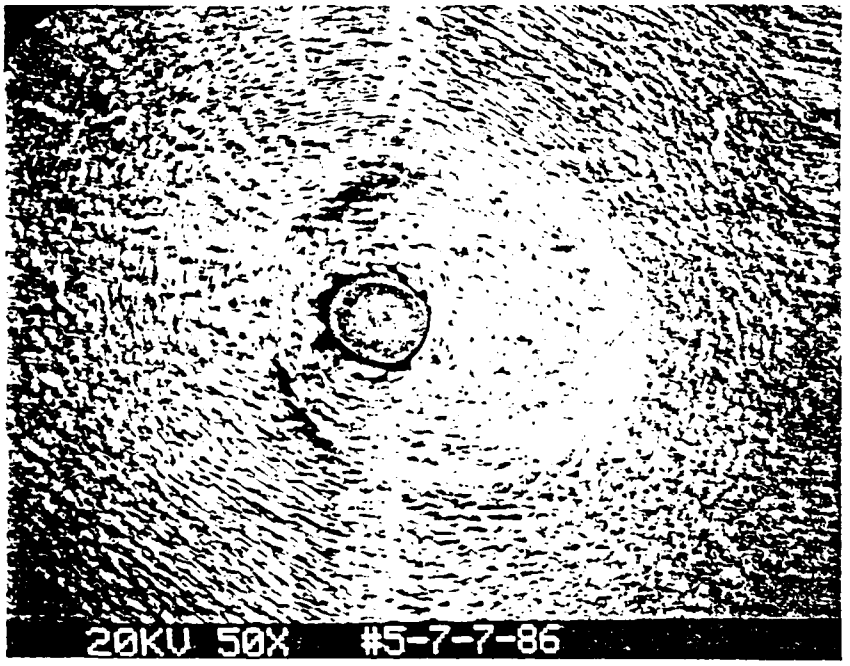

(a)

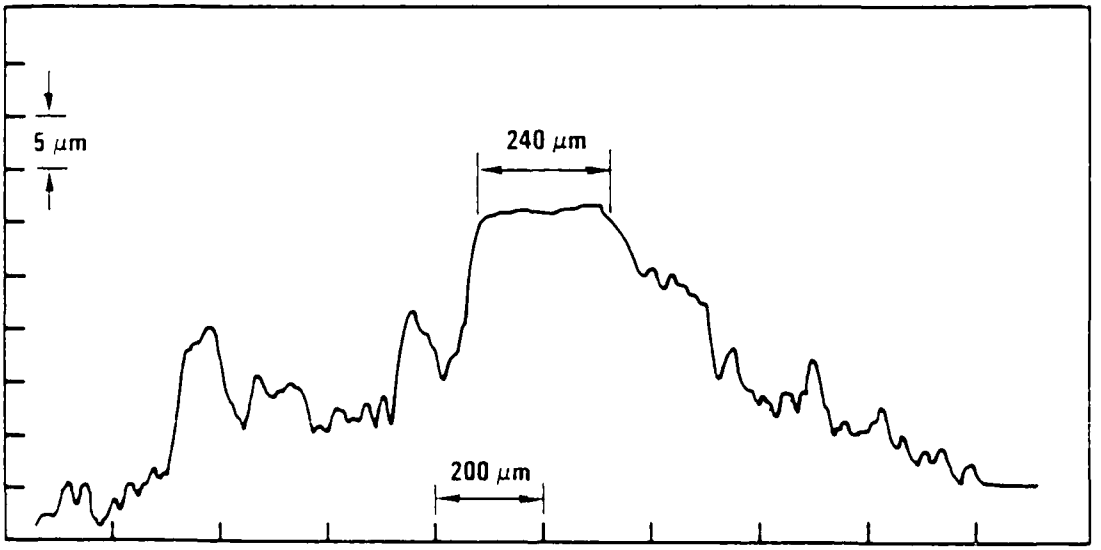

(b)

Fig. 9. (a) SEM photomicrograph and (b) profilometer trace of a laser photochemical produced mesa in *p*-type GaAs.

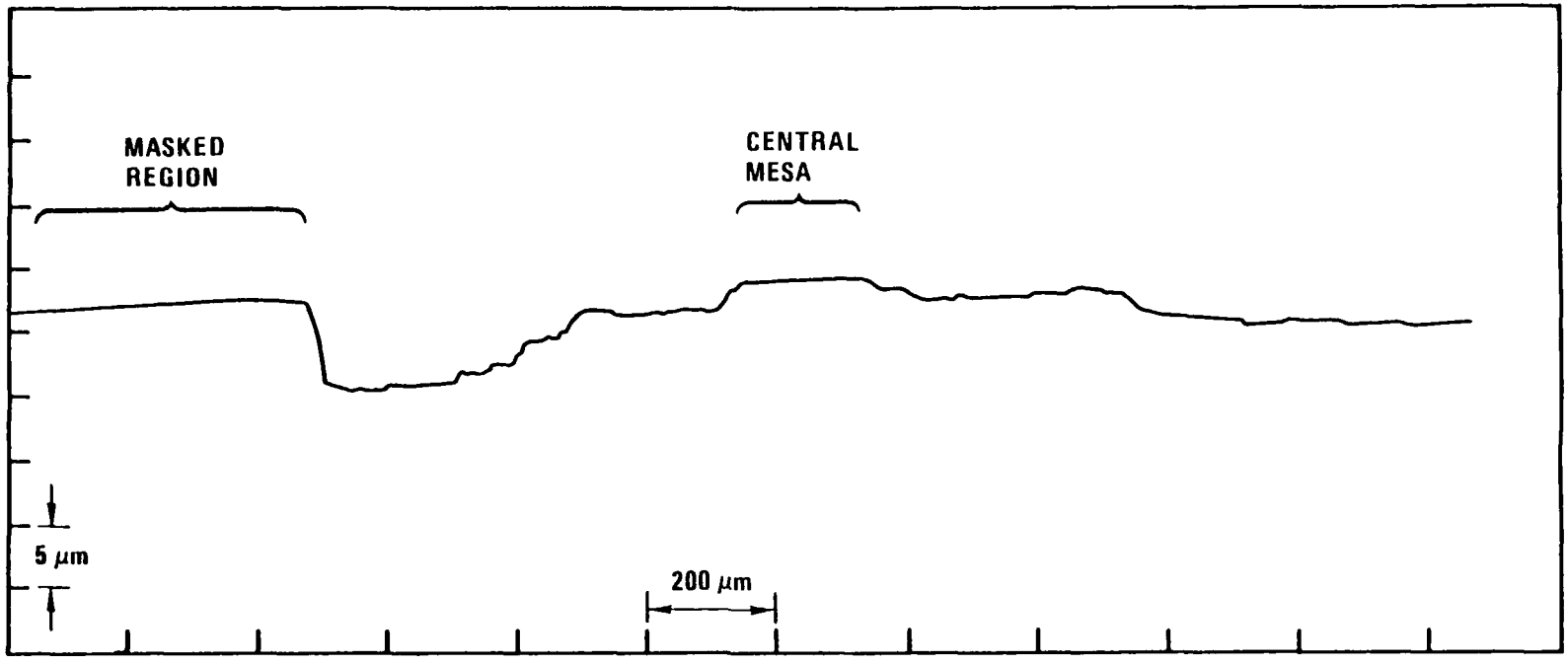

Fig. 10. Profilometer trace of a laser photochemical produced mesa in p-type GaAs.

5. STUDIES ON TPV CELLS

Two types of TPV cells were studied. The first type had p-type stop etch layers as shown in Fig. 11. Results of IR transmission and reflection measurements were encouraging but hole drilling by photoetching in a variety of etchants was unsuccessful. Because of this lack of success, a second batch of cells with an (AlGa)As stop etch layer was made as displayed in Fig. 12. Several cells with holes stopping at the active layers of the cell were finally made by a combination of light and dark etching and contact to the active layers was made in one.

5.1. STUDIES OF TPV CELLS WITH p-TYPE STOP ETCH LAYERS

Many attempts were made at drilling holes in the TPV cells with p-type stop etch layers but all were unsuccessful. However, transmission and reflection measurements proved that a cell with excellent IR reflectivity can be made.

5.1.1. Hole Drilling

Initial attempts to drill holes in TPV cells using the H_2O_2:H_2SO_4:H_2O etchant proved that the thin p-type stop etch layer did not perform as expected from the results on uniformly doped wafers. This seemed to be due to two unfortunate characteristics of the etchant: The rapid dark etching of all types of GaAs and its tendency to decompose and evolve bubbles. This caused two serious problems.

Since the first cells were etched while immersed in a glass beaker, their active layers were protected from dark etching by coating all but a small area on the back

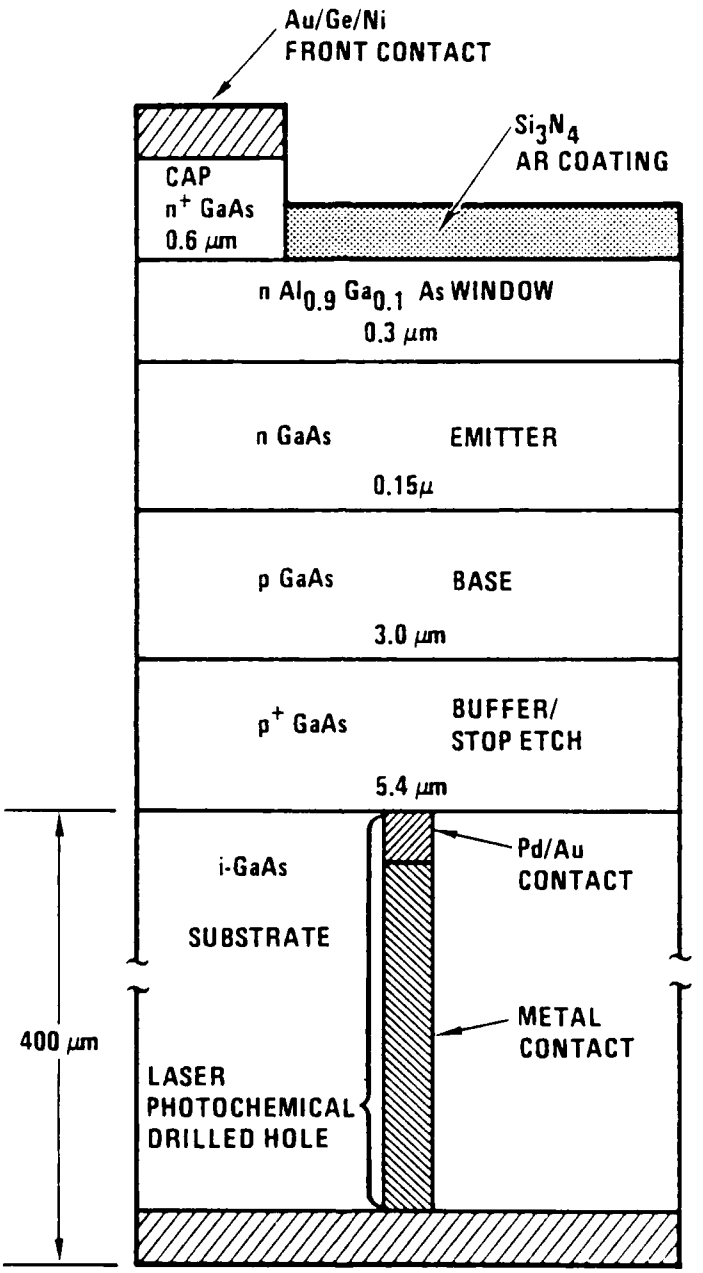

Fig. 11. Schematic of GaAs cell with p-type stop etch layer.

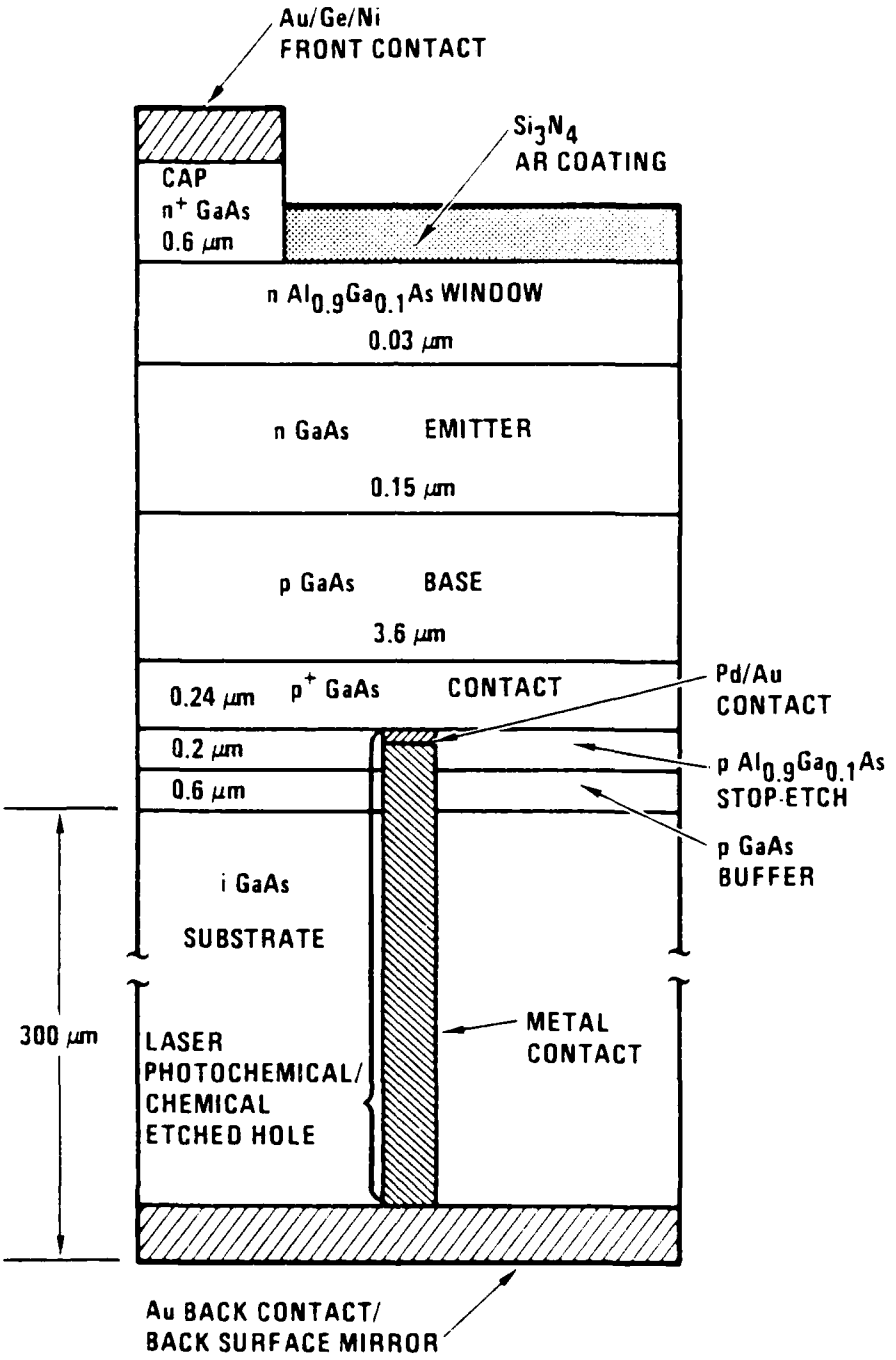

Fig. 12. Schematic of GaAs cell with AlGaAs stop etch layer.

surface of each cell with commercial micromask. But because the solution did not wet it, the surface of the micromask captured bubbles formed on it or on the exposed GaAs. Worse yet, thermal currents due to heating of the solution by the laser beam would draw the bubbles into the beam. Once a bubble got under a beam, it would stay and grow until it both scattered the beam and kept the etchant away from the GaAs. The bubble could be pushed away with a stick, but another would creep under the beam in minutes. This problem was solved by clamping the cell to the bottom of a beaker with a hole in it and eliminating the micromask, as described in the section on experimental methods.

The next problem was more serious. The etching of TPV cells simply did not stop at the stop etch layer. The measured etch rates for the semi-insulating substrate and for bulk *p*-type GaAs agreed very well with those found before (Fig. 7). But when a TPV cell was etched only a few minutes longer than the time required to reach the stop etch layer, the hole either stopped well short of the stop etch layer or went all the way through the cell. The failure of the stop etch layer was probably due to rapid dark etching. The dark etch rate for *p*-type, *n*-type and semi-insulating GaAs was measured by cutting small squares from uniformly doped wafers, coating half of them with micromask and immersing them for hours in the etchant. For the $6.4H_2O_2$:$6.4H_2SO_4$:$100H_2O$ solution and all types of GaAs, the measured dark etch rate was about 1 μm/min. For laser power levels low enough (<3 kW/cm^2) to avoid heating the cell, which would also greatly increase the dark etch rate, the ratio of the photoetch rate to the dark etch rate never exceeded 10. The variation of etch rate from one run to the next was just too large for timing the photoetching well enough. At higher power levels, the bottom of the hole was even melted. The ratio of light etch rate to dark etch rate was found to be even lower for more dilute solutions.

After a thorough literature search [11-16], two other etchants were tried. The first of these was a gold plating solution consisting of 0.5 g of $KAu(CN)_2$ and 10 g of KOH dissolved in 50 cc of H_2O. Results in the literature [13,14] suggested that when

immersed in this solution, *p*-type GaAs would be plated only where illuminated and etched nowhere and *n*-type GaAs would be etched where illuminated and plated in the dark. Furthermore, it appeared that if the semi-insulating substrate were biased positively with respect to an electrode in the solution, the bands could be bent up at the surface so that it would behave like *n*-type GaAs. Since the *p*-type stop etch layer was heavily doped, there should be a range of bias voltages large enough to bend the bands in the semi-insulating GaAs but not large enough to reverse the band bending in the *p*-type GaAs and change its behavior.

First, uniformly doped *p*-type and semi-insulating single crystals were exposed to the plating solution and illuminated as in Fig. 5. Both crystals were plated only where illuminated and neither was etched. Both were examined by scanning electron micrography (SEM) and energy dispersive analysis of x-rays (EDAX) confirmed that the plating was gold. Then, a PAR 173 Potentiostat was connected to a saturated calomel electrode (SCE) and platinum counter electrode in the solution and to the front surface of a TPV cell clamped to a beaker as in Fig. 5. For this purpose, a wire was soldered to the copper block and the cell, which was always mounted front side down, was glued to it with silver paint. The dark I-V curves of a cell and a uniformly doped *p*-type GaAs single crystal were measured this way. The flat band voltage, V_{fb}, the voltage for which I = 0, is just sufficient to reverse the band bending. It was found that V_{fb} = +0.685 V and +1.85 V (versus SCE) for the cell and the *p*-type GaAs respectively. Therefore, a cell was etched with an applied bias of +0.685 V (versus SCE). However, the illuminated area was only roughened and not really etched; there were a few scattered deposits which were proved by SEM and EDAX analysis to be gold. These results seemed to confirm warnings in the literature that photoetching of semi-insulating GaAs in KOH only seems to be stopped by formation of insoluble reaction products [15] and this approach was abandoned.

The best results were obtained with a 5% aqueous solution of nitric acid, which did very little damage to the rest of the cell, though some photoetching of *p*-type GaAs

was observed. For laser powers, P, in the range 1.5 W < P < 2.5 W, corresponding to a range of power densities, S, of 3 kW/cm^2 < S < 5 kW/cm^2 (assuming a spot diameter of 0.010 in), the etch rate was found to be 0.55 to 0.60 (μm/min)/(kW/cm^2). However, illuminating cells for long enough to go through the substrate always produced through holes. This etchant was used in drilling holes in the second type of TPV cells as described later.

5.1.2. Transmission and Reflection Measurements and Comparison to Theory

The transmission of a typical TPV cell with no back surface reflector and of a wafer of intrinsic GaAs the same size and thickness are shown in Fig. 13. As explained in the theory section, the transmission coefficient of a thick dielectric slab is given by

$$T = (1 - R_1)^2 \, x/[1 - R_1 x)^2] \quad , \tag{10}$$

where R is the reflection *coefficient* for the air-dielectric interface and x is given by

$$x = \exp(-\alpha t) \quad , \tag{11}$$

where α is the absorption coefficient and t is the slab thickness. The transmission through the sample holder with no sample was also measured and the results were used to correct the data of Fig. 13. Table 1 shows the values of x calculated from the corrected data and the known reflectance of GaAs [19]. Within our experimental error, no absorption in the intrinsic GaAs could be measured for $\lambda < 14\mu$m. We therefore assumed that all the absorption in the cell was due to the heavily doped active layers and used $t = 8.7\mu$m, the combined thickness of the active layers, to calculated the absorption coefficients in Table 1. The values obtained by this crude approximation are reasonable for doped GaAs [10]. The reflection spectra of a typical TPV cell with a back surface reflector and with the light incident on the front and

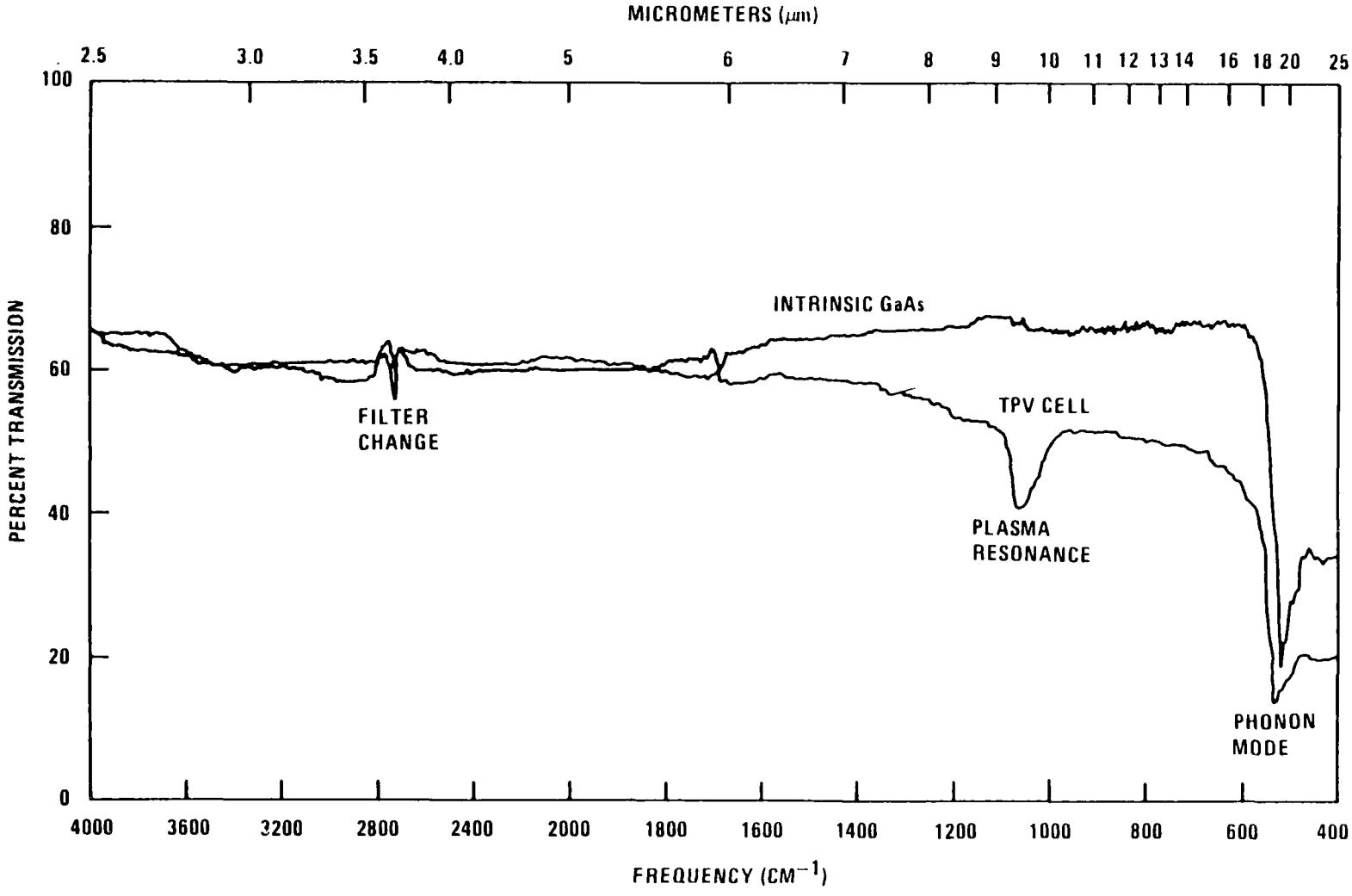

Fig. 13. Infra-red transmission of an intrinsic GaAs single crystal and a TPV cell as shown schematically in Fig. 11.

back of the cell are compared in Fig. 14. Note that the two absorption peaks at $\lambda = 9.4$ and 19μm in the front side reflection spectrum are absent from the back side spectrum. The dip at 9.4μm, which is also present in the transmission spectrum for the TPV cell but absent from the spectrum for intrinsic GaAs in Fig. 13, is probably due to a plasma resonance. The corresponding carrier density can be calculated from [17]

$$\omega_p = e[n/(m^*/m_o)m_o\epsilon\epsilon_o]^{1/2} \quad , \tag{12}$$

where $e = 1.60 \times 10^{-19}$C is the elementary charge, $\epsilon_0 = 8.85 \times 10^{-12}\ F/m$ is the vacuum permittivity, $\epsilon = 13.1$ is the static dielectric constant of GaAs, $m*$ is the effective mass and $m_o = 0.9011 \times 10^{-30}$ kg is the electron rest mass [18]. Using the values $m^*/m_o = 0.45$ and 0.082 gives $n = 10^{20}$ cm^{-3} and 10^{19} cm^{-3} for the heavy and light holes respectively, which agree reasonably well with the expected value for the p-type layers [26]. The dip at 19 μm corresponds to a well known lattice absorption [20,21].

The reflection coefficient of a dielectric slab whose reflection coefficient is R_1 with a back surface reflector with coefficient R_2 with the light incident on the front surface is given by

$$R = R_1 + (1 - R_1)^2\ R_2x^2/(1 - R_1R_2x^2) \quad , \tag{13}$$

where x is given by Eq. (11). Since the reflection coefficient of gold is greater than 0.99 for $2.0\mu\text{m} < \lambda < 25\mu$m [22], the reflection coefficient of the cell was taken to be

$$R = R_f/R_b \quad , \tag{14}$$

where $R_f(R_b)$ is the measured reflection with the light incident on the front (back) surface. The reflection coefficient of the back surface reflector, R_2, was calculated from

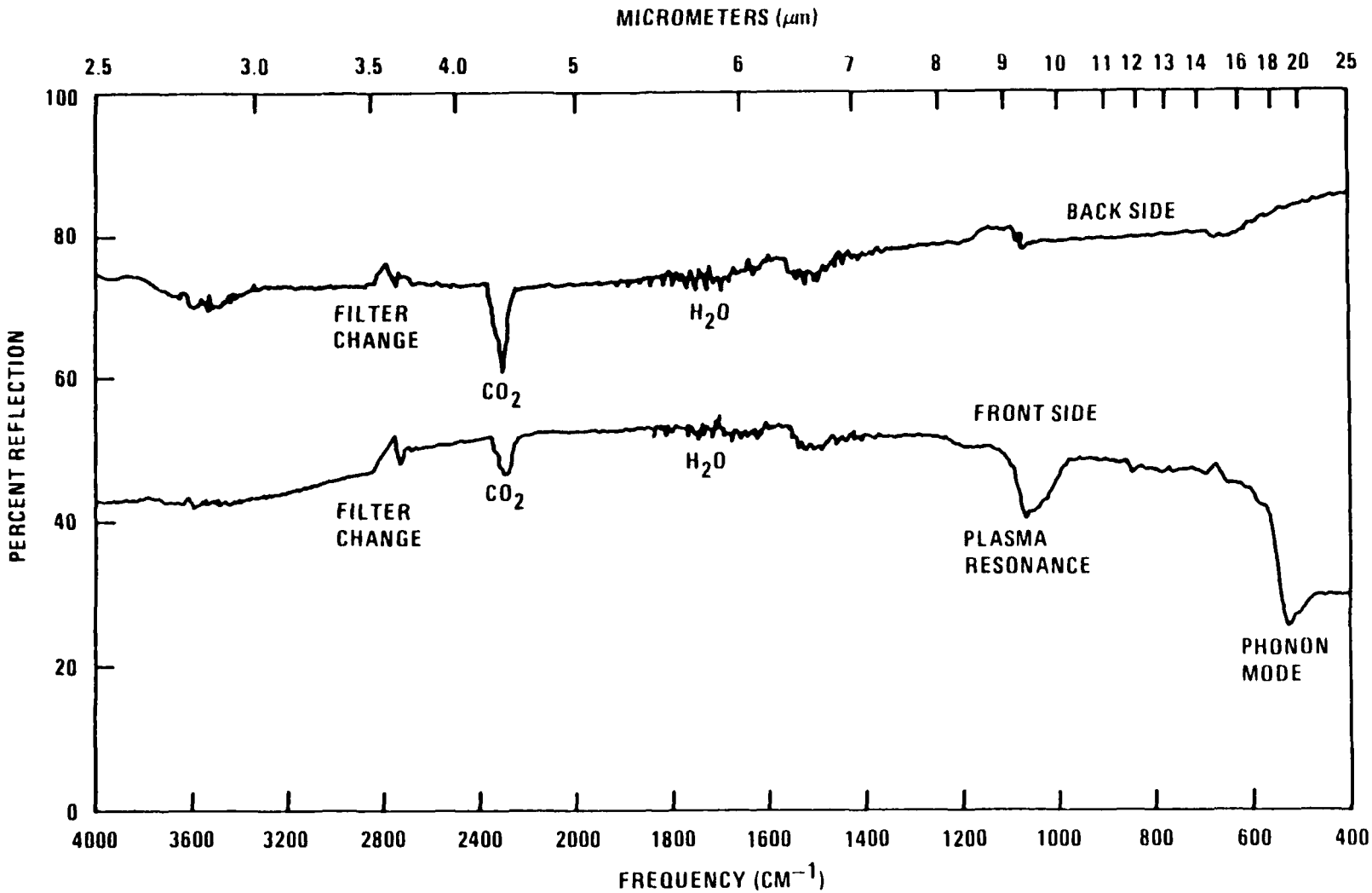

Fig. 14. Infra-red reflection off of the front surface and the back surface of a TPC cell as shown schematically in Fig. 11.

Table 1

IR ABSORPTION COEFFICIENTS FOR INTRINSIC GaAs AND TPV CELLS

$\lambda(\mu m)$	R_1	x_i	x_c	$\alpha_c(cm^{-1})$
3.0	0.289	1.0	1.0	0
4.0	0.289	1.0	0.99	7
5.0	0.289	1.0	0.98	24
8.0	0.289	1.0	0.90	120
9.0	0.287	1.0	0.83	210
11.0	0.285	1.0	0.82	230
14.0	0.285	1.0	0.80	260

R_1 = reflectance of GaAs-air interface [19], $x \equiv \exp(-\alpha t)$ where α = absorption coefficient and t = thickness. Subscripts i and c refer to intrinsic GaAs and TPV cell respectively.

the measured value of R, the value of x_c from transmission measurements (Table 1) and the known values of R_1 and the results are shown in Table 2. The correction to R_1 due to the Si_3N_4 antireflection coating (Fig. 11), which is optimized for the wavelength corresponding to the bandgap, $\lambda_g = 0.9\mu m$, was estimated to be too small to change these results.

5.2. STUDIES OF TPV CELLS WITH AlGaAs STOP ETCH LAYERS

The second type of TPV cells (Fig. 12) were almost the same as the first (Fig. 11) except that the stop etch layer was $Al_{0.9}Ga_{0.1}As$ instead of p-GaAs. As we expected, we were able to drill a hole most of the way through the substrate by photoetching in nitric acid and then finish the hole by dark etching.

Table 2

REFLECTANCE OF TPV CELL WITH BACK SURFACE REFLECTOR

$\lambda(\mu m)$	R	R_1	x_c	R_2
3.0	0.60	0.289	1.00	0.53
4.0	0.69	0.289	0.99	0.67
5.0	0.63	0.289	0.98	0.59
8.0	0.66	0.289	0.90	0.75
9.0	0.62	0.287	0.83	0.79
11.0	0.62	0.287	0.82	0.82
14.0	0.59	0.285	0.80	0.80

R = measured reflectance of TPV cell; R_1 = known reflectance of air-GaAs interface [19]; $x_c = \exp(-\alpha_c t)$ is taken from Table 1; R_2 = reflectance of back surface reflector calculated from Eq. (13).

5.2.1. Chemical Selectivity

There are several etchants for (AlGa)As whose etch rate depends strongly on the aluminum content. In particular, optical devices have been made by etching all or a portion of a GaAs substrate with an AlGaAs epitaxial layer in NH_4OH:H_2O_2 [23-25]. In fact the selectivity defined by

$$S = S_1/S_2 \quad , \tag{15}$$

where S_1 and S_2 are the rate of etching of GaAs and AlGaAs has been found to be as high as 30 [24]. It is also known [26] that a buffered oxide etch of HF:NH_4F will remove AlGaAs without attacking GaAs.

5.2.2. Hole Drilling

Holes about 240 microns deep were drilled in the 300 micron thick Cr-doped semi-insulating substrates of the TPV cells by etching in a 5% (volume) aqueous solution of HNO_3 with the assistance of a 1.5 W beam from an argon ion laser operating on all lines (Fig. 5). The beam was focused down to a spot about 250 microns in diameter so that the power density on the surface of the GaAs was about 300 W/cm^2. A typical hole is shown in Fig. 15. The hole is roughly elliptical and the ratio of the major to the minor radius grows with increasing depth; this indicates anisotropic etching. A thin film, probably of oxide, surrounds the hole for about three times the hole diameter. The hole was then dark etched in an ultrasonically agitated solution using the apparatus shown in Fig. 6. The purpose of the first dark etch in H_2O_2:NH_4OH was to etch the remaining ~60 microns of GaAs down to the AlGaAs stop-etch layers. The cell was tied down to a glass microscope slide with teflon tape, without which the bubbles from the peroxide would have caused the cell to float in the solution, and all but a small area around the hole was painted with micromask. After about 30 minutes of etching, the bottom of the hole was flat and bluish green; the color indicates that the bottom is covered with oxidized (Al,Ga)As [26]. The depth of the hole was about 300 microns below the unetched back surface.

The cell was then dark-etched in the buffered oxide etch HF:NH_4F to remove the AlGaAs stop-etch layer and etch down to the p^+ contact layer which is not attacked by this etchant. After about 30 minutes, the bottom of the hole was almost cleared of film as shown in Fig. 16. One cell was metallographically potted and sectioned to expose the cross-section of the final hole. A series of scanning electron micrographs are shown in Fig. 17. These photomicrographs clearly show that a hole was etched through the GaAs substrate to the p^+ contact layer where the etching was stopped

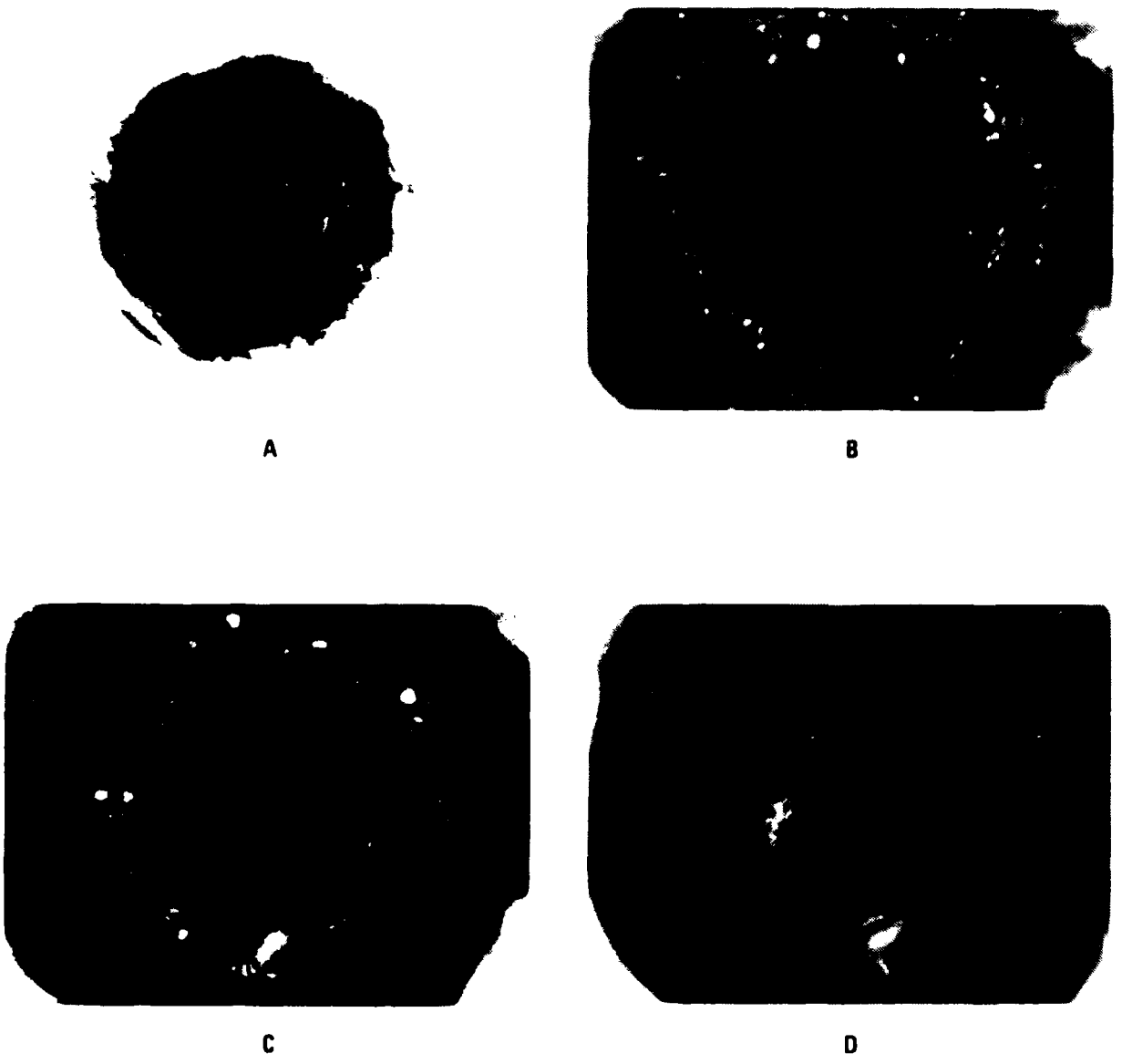

Fig. 15. Photomicrographs of a hole etched in SI-GaAs using a laser photochemical technique, focused at distances from the entrance of the hole of (a) 0 μm (120X); (b) 35 μm (240X); (c) 67 μm 240X; (d) 130 μm (240X).

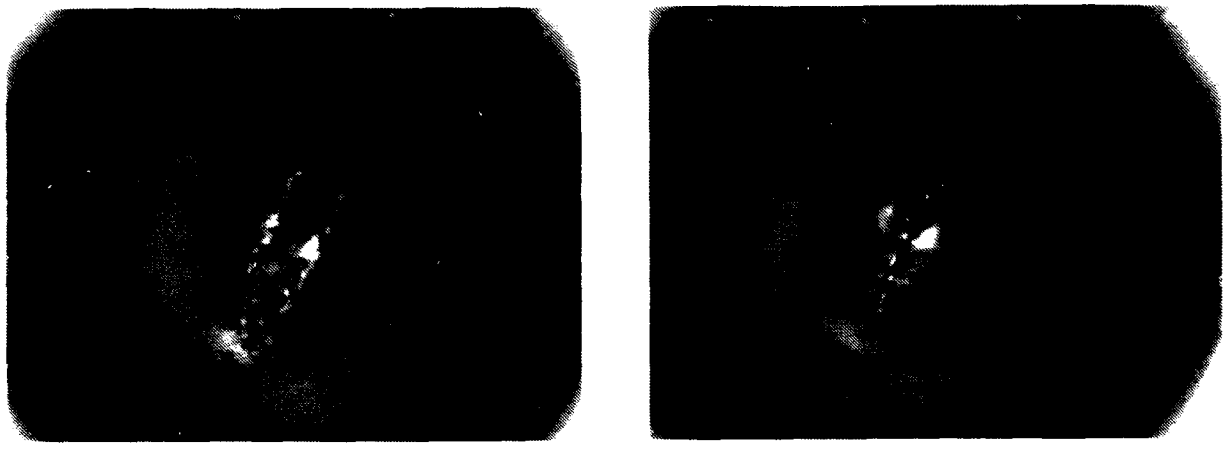

E F

G

Fig. 15. Photomicrographs of a hole etched in SI-GaAs using a laser photochemical technique, focused at distances from the entrance of the hole of (e) 200 μm (240X); (f) 220 μm (240X); (g) 230 μm (240X).

Fig. 16. Area of bottom of hole after laser and dark etching to the p^+ GaAs contact layer of a cell schematically shown in Fig. 12 (240X).

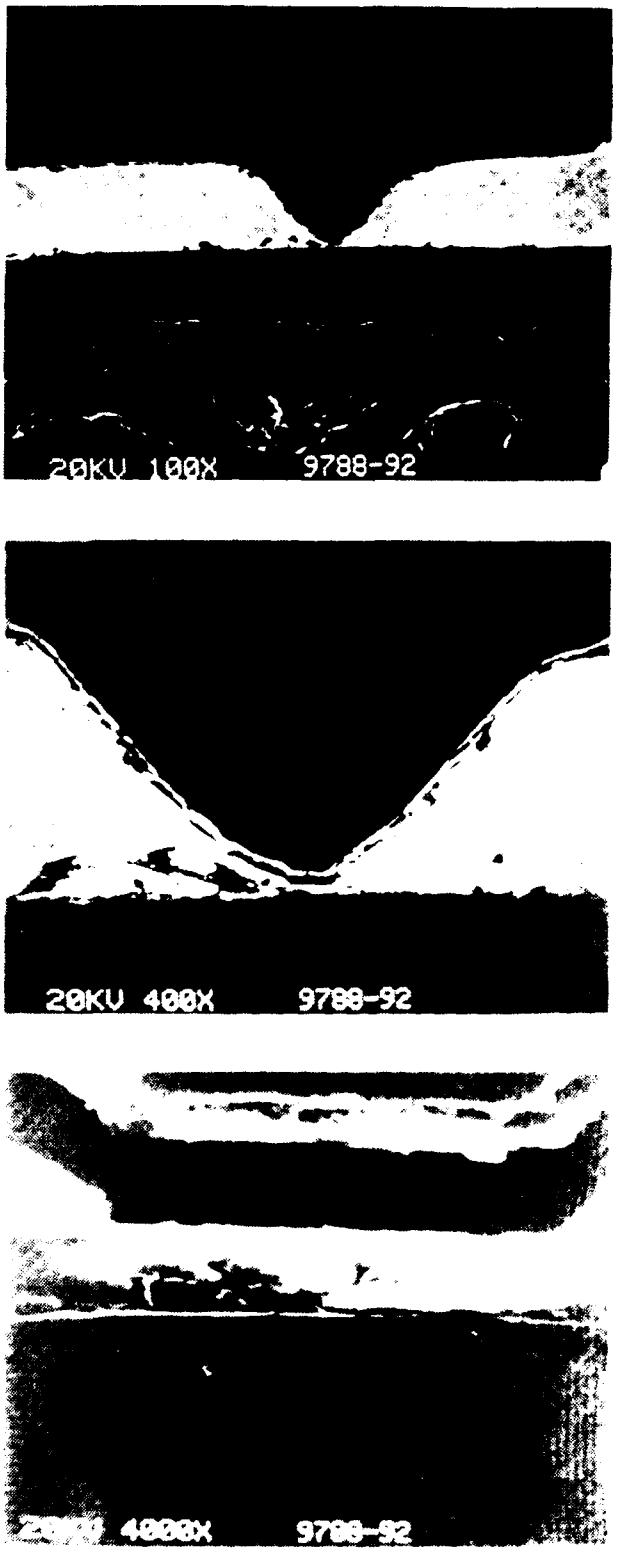

Fig. 17. Scanning electron photomicrograph of a metallographically mounted GaAs cell, shown schematically in Fig. 12. In the 4000X photomicrograph, the pullout between the potting compound and the cell is evident.

5.2.3. IR Reflection

Varian Associates assisted in the preparation of four non-etched cells and one cell with an etched hole for IR reflectivity measurements by removing the cap layer from between the front surface contacts using a proprietary etch (see Fig. 12), depositing a Pd/Au ohmic contact at the base of the etched hole, and then coating the back surface of the etched cell with gold. This coating filled up the etched hole with gold. In addition, a gold coating was evaporated on the back surface of four non-etched cells. The reflectivity of both etched and non-etched cells was then measured from 2.5 to 25 microns with the radiation normally incident on the front and back surface. Similar IR reflectivity results were obtained for both the etched and non-etched cells. As shown in Fig. 18, the spectra are very similar to those for the TPV cells with p-type stop etch layers; the front surface reflectivity of the intact cells was about 60% of the back surface reflectivity over most of the frequency range. These cells lacked an anti-reflection coating, which, if applied, would not have modified these results.

5.2.4. I-V Characteristics

The dark, forward I-V characteristic of cell 9788-96 which had a hole stopping at the active layers, which were filled with gold, and a gold back contact is shown in Fig. 19. While the log current versus voltage plot was not linear, an activated diode-like current-voltage characteristic is evident, indicating that the $p-n$ junction had not been compromised by the etching. A significant series resistance of a few hundred ohms is apparent from the data. This might have arisen from the small contact area of the Pd/Au with the p^+ GaAs contact layer or to the lack of an anneal after the Pd/Au deposition. In addition, this particular cell had a very thin gold top contact ($\sim$few hundred $\AA$) which also would contribute to a substantial series resistance. It is likely that all the above contributions to the series resistance could be readily eliminated, leading to a cell with low series resistance and high IR reflectivity.

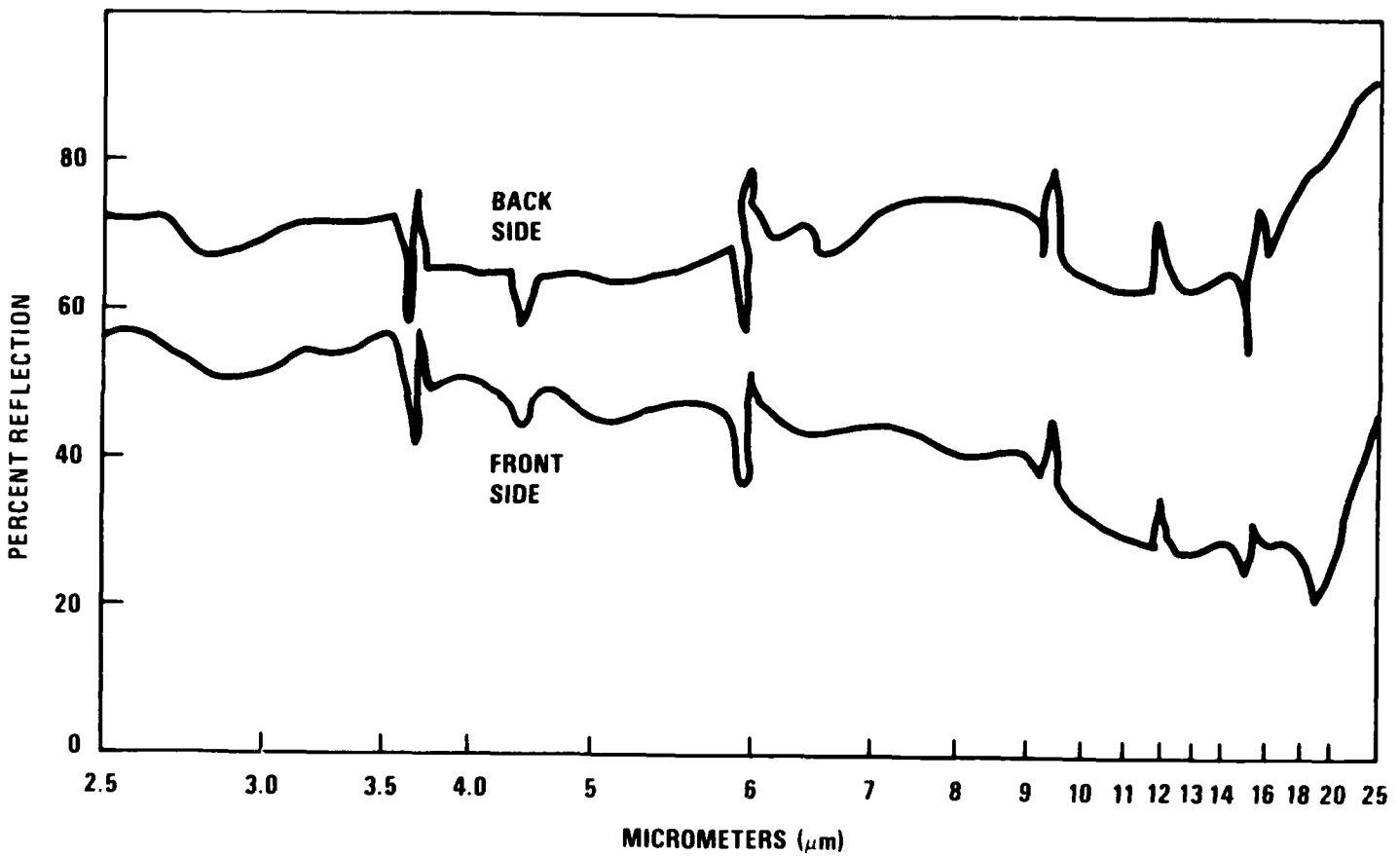

Fig. 18. IR reflectivity data from both the front and back surface of a non-etched TPV cell, shown schematically in Fig. 12.

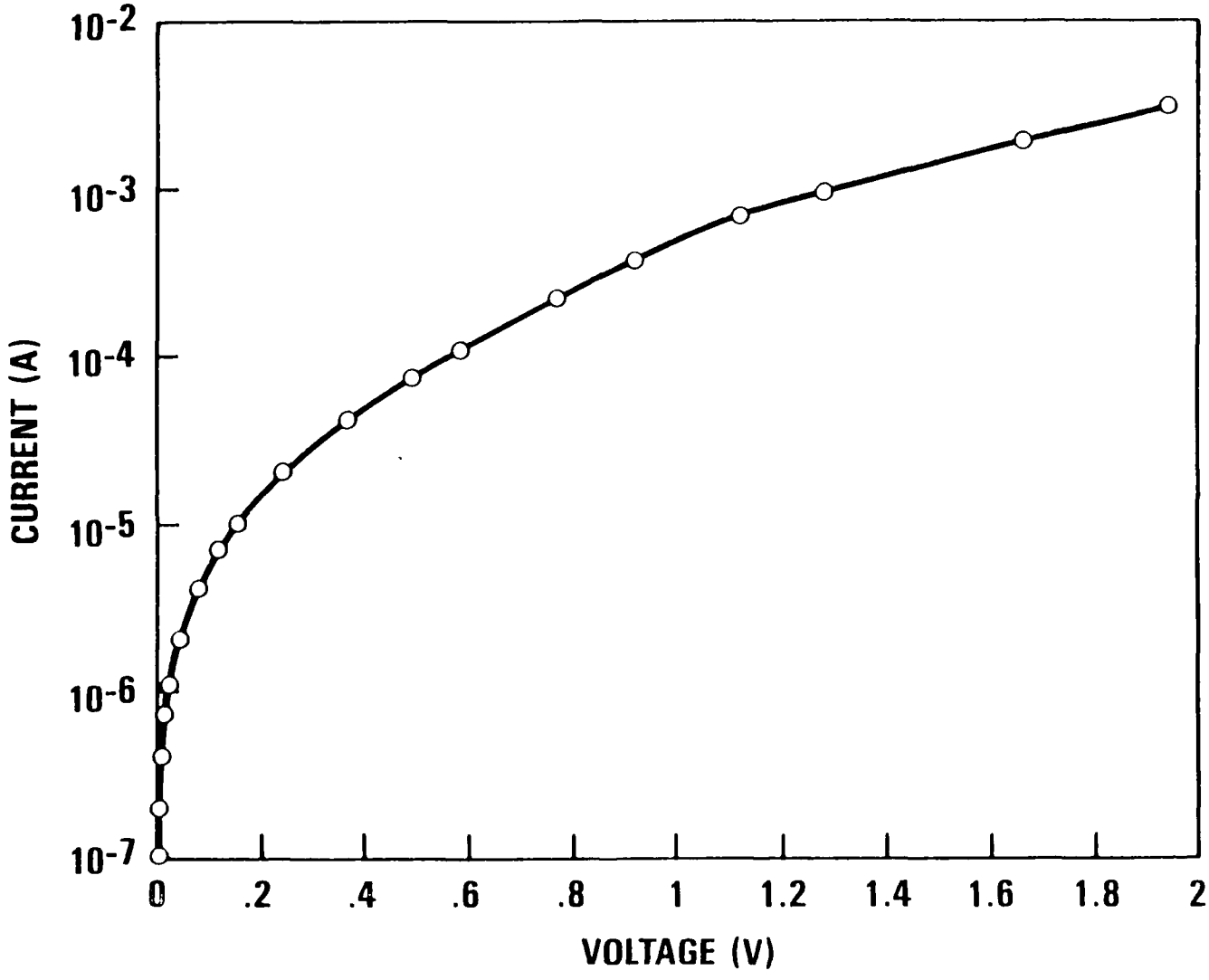

Fig. 19. Dark current versus voltage characteristic for a cell, shown schematically in Fig. 12, in which an etched hole in Si-GaAs was filled with gold.

6. APPLICATION OF TPV CELL DATA TO TPV SYSTEM EFFICIENCY

As shown in Figs. 13, 14 and 18, the infra-red (IR) reflectivity of the GaAs TPV cells tested exceeded 70%, corresponding to a weighted parasitic absorption of ~0.3 or less. It should be pointed out that the exact correlation between the weighted parasitic absorption $\overline{A}_{par}$ and the IR reflectivity depends on the TPV cell band gap and the blackbody absorber/emitter temperature. Previous theoretical treatments have examined the relationship between the $\overline{A}_{par}$ and the TPV efficiency [1,2]. Presented in Fig. 20 is a plot of the optimum TPV efficiency and associated optimum band gap versus $\overline{A}_{par}$ for a blackbody absorber/emitter temperature of 2100 K and a TPV cell temperature of 300 K. For $\overline{A}_{par} = 0.3$, the optimum efficiency is ~22% and the optimum band gap is ~0.75 eV.

It is likely that TPV cells with reflectivities approaching 95% between 1 and 10 microns (corresponding approximately to $\overline{A}_{par} = 0.05$) can be fabricated, based on the cell data shown in Table 1. Then, Fig. 20 would imply that TPV efficiencies exceeding 35% would be feasible.

Plots of the TPV efficiency as a function of cell temperature for commercially available research concentrator InGaAs cells with band gaps of 1.15 and 1.2 eV, GaAs cells and Si cells are shown in Figs. 21 and 22 [1]. These data were calculated using a model previously described [1], based on measured dark current versus voltage characteristics as a function of temperature and assuming $\overline{A}_{par} = 0.05$. The IR reflectivity data for a GaAs cell imply that a value of $\overline{A}_{par}$ as low as 0.05 is attainable. These figures, then, indicate the efficiencies that are likely to be achieved using commercially available cells which have been modified for high below band gap reflectivity.

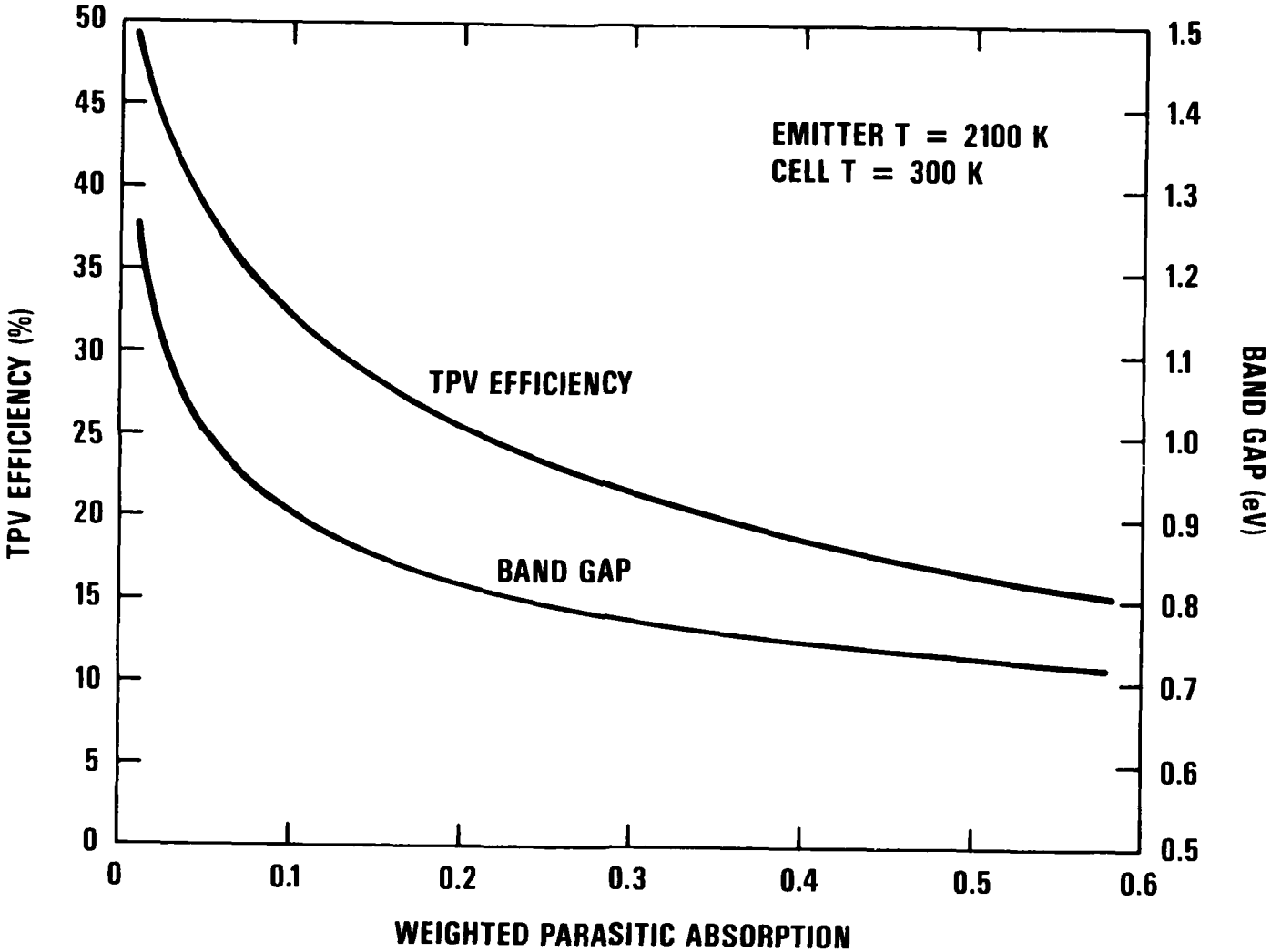

Fig. 20. Optimum TPV efficiency and associated band gap versus weighted parasitic absorption $\overline{A}_{par}$ for an emitter temperature of 2100 K and a cell temperature of 300 K [1,2].

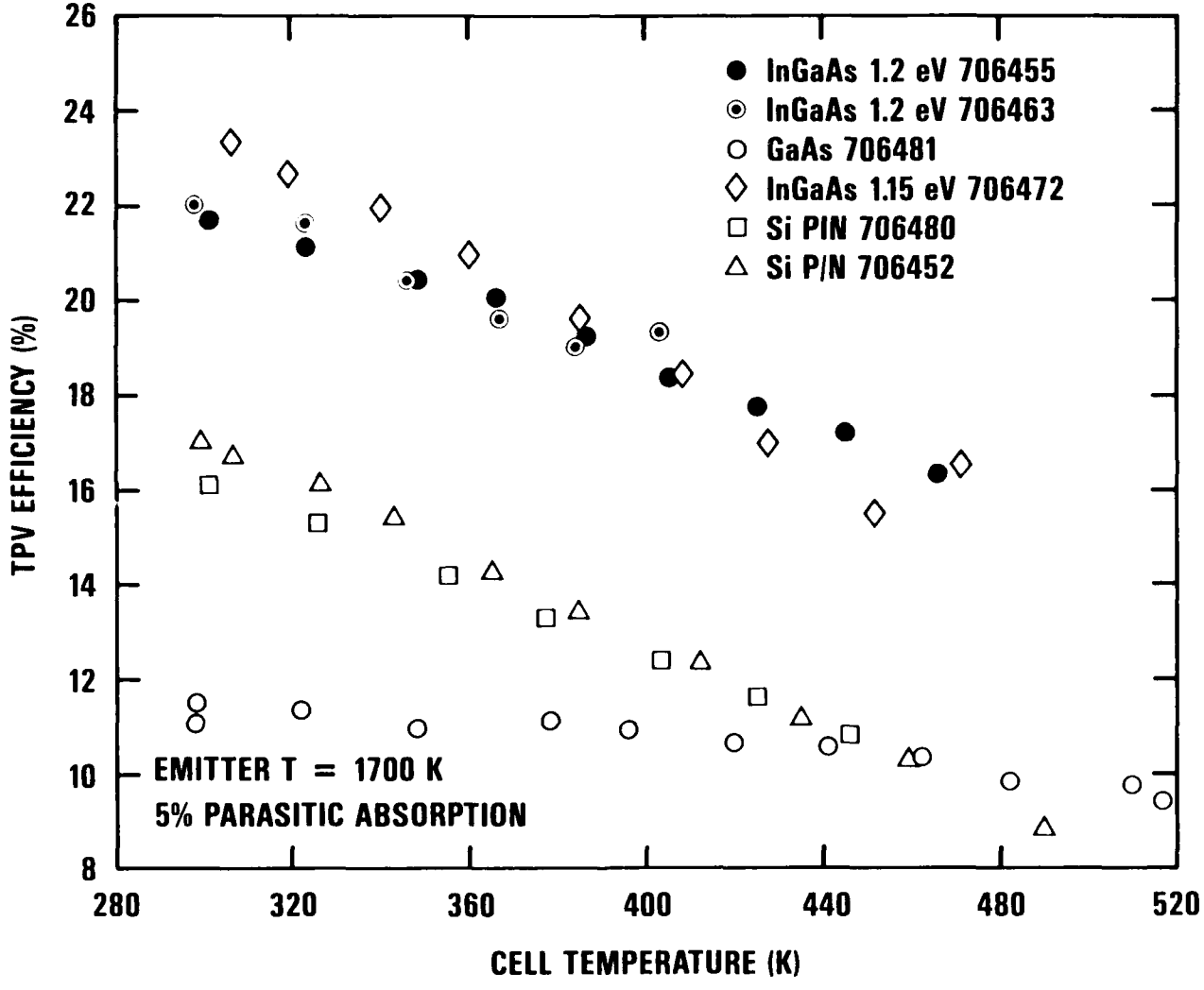

Fig. 21. Calculated TPV efficiency versus cell temperature for an emitter temperature of 1700 K [1].

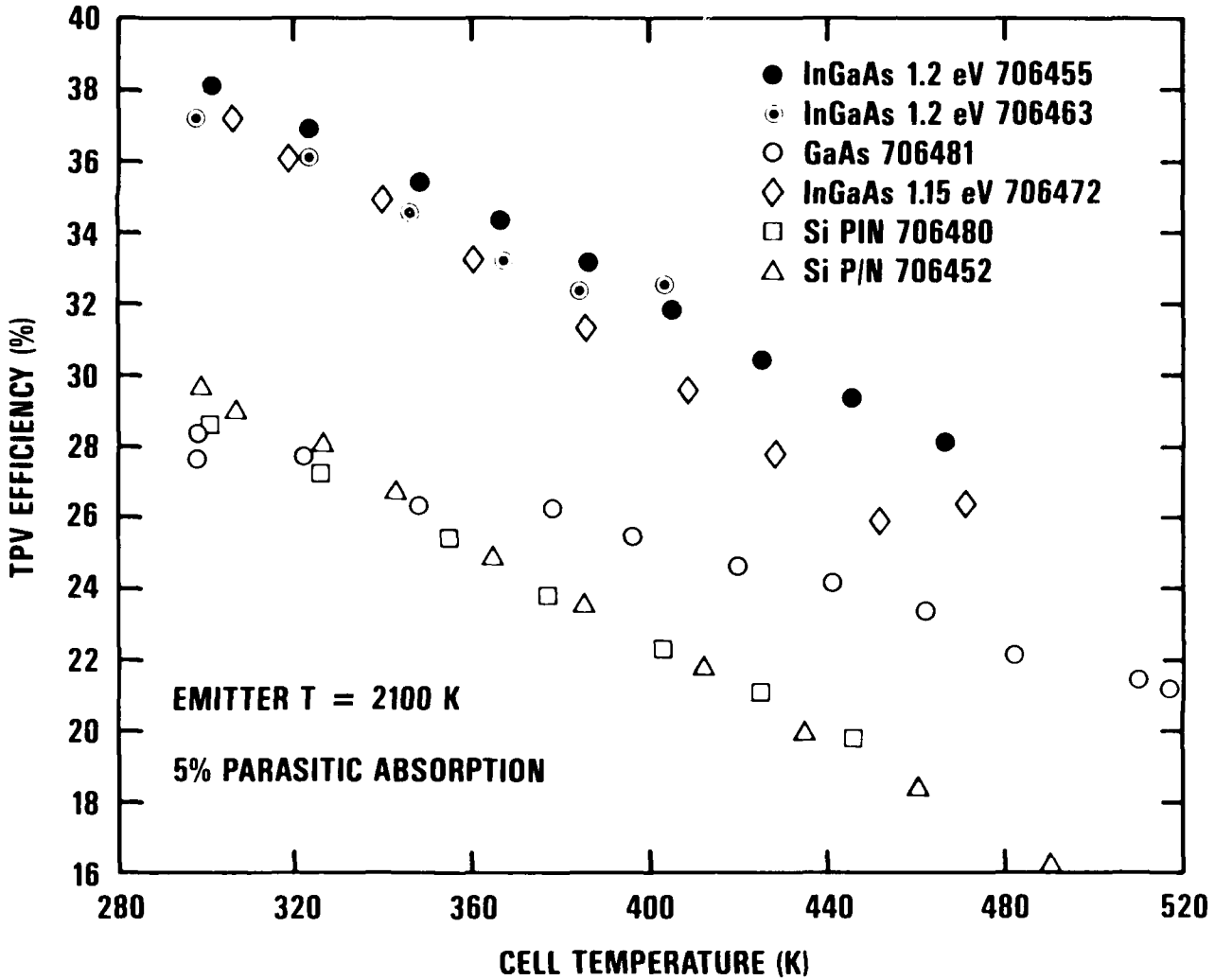

Fig. 22. Calculated TPV efficiency versus cell temperature for an emitter temperature of 2100 K [1].

7. RECOMMENDATIONS FOR APPLICATIONS OF THIS TECHNOLOGY

This research has indicated that it is feasible to fabricate GaAs based cells which are greater than 70% reflective in the below band gap energy regime. If the reflectivity can be increased to ~90% while maintaining a low cell series resistance, corresponding to ~10% weighted parasitic absorption, then thermophotovoltaic conversion efficiencies in excess of 35% would appear to be practical. The absorber/emitter must also efficiently absorb and emit photons so as not to degrade the thermophotovoltaic efficiency. A detailed analysis of absorber/emitter design requirements and materials development has not been addressed in this study.

One prime area for the application of this technology is in high efficiency solar energy conversion. Solar energy conversion efficiencies in excess of 30% will be required for future defense and NASA missions. By coupling a high efficiency GaAs or InGaAs TPV cell with a high-efficiency emitter/absorber and TPV cavity, such efficiencies would appear to be attainable. In addition, since the absorber/emitter is in the optical pathway between the focusing optics and the TPV cell, the energy conversion system may be significantly hardened against external harmful sources of electromagnetic radiation and particles. High efficiency cells also allow for high efficiency solar photothermophotovoltaic (PTPV) systems [27,28], which have advantages over comparable TPV and photovoltaic systems. However, required cavity design studies have not yet been carried out for solar PTPV systems, whereas they have been performed for solar TPV systems [29]. Such design studies would be required for a realistic assessment of PTPV systems.

Another potential application of this technology would be in nuclear thermophotovoltaic energy conversion [3] for a space-based system with ~10 kW electrical output. For systems with ~100 to 1000 kW electrical output, the radiator mass dominates over other masses. Since specific power (watts/kg) is of prime importance in space-based systems, the low radiator temperature of ~500 to 600°K for a nuclear TPV system compared to ~700°K for a thermoelectric and ~1000°K for a thermionic system would lead to unreasonably large radiator masses for the nuclear TPV system. However, for relatively low electrical output systems of ~10 kW, the radiator mass will not be as dominant and high energy conversion efficiency becomes a more dominant contribution to the specific mass. Since TPV energy conversion efficiencies can be as high as 30 to 40%, considerably higher than either thermoelectrics or thermionics, this technology should seriously be considered. Although a detailed design has not been performed, it is probable that a nuclear-TPV system with reactor and heat pipes compatible with the current SP-100 nuclear thermoelectric system (absorber/emitter temperature of ~1350 to 1400°K) would have a specific power greater than or equal to that of a thermoelectric-based system.

Two other potential applications of this technology should also be considered. First, a space-based TPV system heated using a radioisotope heat source might prove to be considerably more efficient than the conventional thermoelectric-based system, particularly for systems in ranges of ~3 to 10 kW of electrical power. Second, conventional solar cells, particularly those based on GaAs, which operate under concentrated sunlight are heated, in part, because of their high absorptivity for below band gap energy photons. GaAs solar cells based on the shorted substrate cell approach with back surface mirrors would operate at a much lower temperature (~50 to 100°C) than standard GaAs cells since they would reflect nearly all the infra-red energy back to space. Furthermore, shorted substrate cells with no back surface reflector would be nearly transparent to below band gap energy radiation and could be used as the top cell in a stacked multiple band gap cell.

8. RECOMMENDATIONS FOR CONTINUED WORK

A method for fabricating the shorted substrate GaAs-based cell has been identified by this research. However, the morphology of the hole through the substrate was quite non-circular, and the contact area at the GaAs contact layer appears to have been quite small, contributing to a larger than expected cell series resistance. Therefore, it is recommended that three methods be considered for further shorted substrate cell development:

- Further development of the method described in this report, which used a combined laser photochemical/chemical etch.
- Development of alternative hole drilling methods in fully grown GaAs-based cells.
- Development of hole drilling methods prior to cell growth and epitaxial growth of the cells over these open holes.

Further efforts should focus on enhancing the reflectivity of the back surface mirror and on reducing the cell series resistance by either increasing the area of the holes and/or by developing superior ohmic contact fabrication methods. Finally, measurements of the cell reflectivity and series resistance as a function of temperature will be required, since TPV cells will likely operate at elevated temperatures of 500 to 600 K in many possible space-based energy conversion systems.

9. REFERENCES

[1] L. D. Woolf, J. C. Bass and N. B. Elsner, "Variable Band Gap Materials for Thermophotovoltaic Generators," GA Technologies Report GA-A18140, September 1985.

[2] L. D. Woolf, *Solar Cells*, **19**, 19 (1986-1987).

[3] J. C. Bass, *et al.*, "Nuclear-Thermophotovoltaic Energy Conversion," NASA Report CR-167988, GA Technologies Report GA-A16653, December 1983.

[4] R. J. Boettcher, *et al.*, Proc. 16th IEEE Photovoltaic Specialists Conference, p 1470 (1982).

[5] J. C. C. Fan, C. O. Bozler, Rand R. W. McClelland, Proc. 15th IEEE Photovoltaic Specialists Conference, p 666 (1981).

[6] H. Gerischer, *J. Vac. Sci. Technol*, **15**, 1422 (1978); S. R. Morrison, *Electrochemistry at Semiconductor and Oxidized Metal Electrodes*, Plenum Press, New York, 1980.

[7] S.-M. Park and M. E. Barber, *J. Electroanal. Chem.*, **99**, 67 (1975).

[8] F. W. Ostermayer, Jr., and P. A. Kohl, *Appl. Phys. Lett.*, **39**, 76 (1981); H. Gerischer, in *Physical Chemistry, An Advanced Trestise*, ed. H. Eyring (Academic, New York, 1970), Vol. IXA, Chap. 5, p 530.

[9] F. Kuhn-Kuhnenfeld, *J. Electrochem. Soc.*, **119**, 1063 (1972).

[10] W. T. Spitzer and J. M. Whelan, *Phys. Rev.*, **114**, 59 (1959).

[11] D. V. Podlesnik, H. H. Gilgen and R. M. Osgood, Jr., *Appl. Phys. Lett.*, **45**, 563 (1984).

[12] C. I. H. Ashby in *Properties of Gallium Arsenide*, ed., J. S. Blakemore, INSPEC, New York, 1986.

[13] R. W. Haisty, *J. Electrochem. Soc.*, **108**, 790 (1961).

[14] R. H. Micheels, A. D. Darrow, II, and R. D. Raub, *Appl Phys. Lett.*, **39**, 418 (1981).

[15] G. C. Tisone and A. W. Johnson, *Appl. Phys. Lett.*, **42**, 530 (1983).

[16] P. A. Kohl, C. Wolowodiuk and F. W. Ostermayer, Jr., *J. Electrochem. Soc.*, **130**, 2288 (1983).

[17] R. A. Smith, *Semiconductors*, 2nd ed., Cambridge University Press, London, 1978, p 302.

[18] S. M. Sze, *Physics of Semiconductor Devices*, 2nd ed., John Wiley and Sons, New York, 1981.

[19] B. O. Seraphim and H. E. Bennett in *Optical Properties of III-V Compounds*, v. 3 of *Semiconductors and Semimetals*, ed. R. K. Willardson and A. C. Beer, Academic Press, New York 1967.

[20] W. G. Spitzer in *Optical Properties of III-V Compounds*, v. 3 of *Semiconductors and Semimetals*, ed. R. K. Willardson and A. C. Beer, Academic Press, New York 1967.

[21] M. R. Brozel in *Properties of Gallium Arsenide*, ed. J. S. Blakemore, INSPEC, New York, 1986.

[22] *CRC Handbook of Chemistry and Physics*, 67^{th} ed., R. C. Weast, Boca Raton, 1986.

[23] J. L. Jewell, H. M. Gibbs, A. C. Gossard, A. Passner and W. Wiegmann, *Matl. Lett*, to be published.

[24] J. J. LePore, *J. Appl Phys.*, **51**, 6441 (1980).

[25] R. A. Logan and F. K. Reinhart, *J. Appl. Phys.*, **44**, 4172 (1973).

[26] J. Werthen, Varian Associates, private communication.

[27] L. D. Woolf, Proc. 19th IEEE Photovoltaic Specialists Conference (1987).

[28] L. D. Woolf, Proc. 22nd International Energy Conversion Engineering Conference, p 88 (1987).

[29] W. E. Horne, A. C. Day and L. Crabtree, Proc. 17th International Energy Conversion Engineering Conference, p 119 (1982).

10. LIST OF PROFESSIONAL PERSONNEL ASSOCIATED WITH THE RESEARCH EFFORT

Dr. Lawrence D. Woolf	Staff Scientist/Principal Investigator
Dr. Dennis M. Duggan	Senior Scientist
Dr. Joe N. Smith, Jr.	Staff Scientist
Dr. Hal Streckert	Senior Scientist

11. LIST OF WRITTEN PUBLICATIONS IN TECHNICAL JOURNALS AND CONFERENCE PROCEEDINGS

Based on work performed under AFOSR Contracts F49620-86-C-0043 and F49620-84-C-0105.

1. Woolf, L.D., "Optimum Efficiency of Single and Multiple Band Gap Cells in Thermophotovoltaic Energy Conversion," *Solar Cells*, **19**, 19 (1986-1987).

2. Woolf, L.D., "Optimum Efficiency of Single and Multiple Band Gap Cells in TPV Energy Conversion," *Proc. 18th IEEE Photovoltaic Specialists Conference*, p 1731 (1985).

3. Woolf, L.D., J.C. Bass and N.B. Elsner, "Theoretical and Experimental Investigation of Variable Band Gap Cells in Thermophotovoltaic Energy Conversion," *Proc. 32nd International Power Sources Symposium*, p 101 (1986).

4. Woolf, L.D., J.N. Smith, Jr., and D.M. Duggan, "High Efficiency GaAs-Based Cells for Thermophotovoltaic Generators," *Proc. 22nd International Energy Conversion Engineering Conference*, p 264 (1987).

12. LIST OF PAPERS OR POSTERS PRESENTED AT CONFERENCES

Based on work performed under AFOSR Contracts F49620-86-C-0043 and F49620-84-C-0105.

1. Woolf, L.D., "Optimum Efficiency of Single and Multiple Band Gap Cells in Thermophotovoltaic Energy Conversion," post-deadline poster presented at the 18th IEEE Photovoltaic Specialists Conference, 1985.

2. Woolf, L.D., J.C. Bass and N.B. Elsner, "Theoretical and Experimental Investigation of Variable Band Gap Cells in Thermophotovoltaic Energy Conversion," paper presented at the 32nd International Power Sources Symposium, 1986.

3. Woolf, L.D., J.N. Smith, Jr., and D.M. Duggan, "High Efficiency GaAs-Based Cells for Thermophotovoltaic Generators," paper presented at the 22nd International Energy Conversion Engineering Conference, 1987.

13. LIST OF WRITTEN PUBLICATIONS RELATED TO THERMOPHOTOVOLTAICS IN CONFERENCE PROCEEDINGS

Based on work performed under GA Technologies Inc. Internal Research and Development Funds.

1. Woolf, L.D., "Solar Photothermophotovoltaic Energy Conversion," Proc. 19th IEEE Photovoltaic Specialists Conference (1987).

2. Woolf, L.D., "Solar Photothermophotovoltaic Energy Conversion," Proc. 22nd International Energy Conversion Engineering Conference, p 88 (1987).

14. LIST OF PAPERS OR POSTERS RELATED TO THERMOPHOTOVOLTAICS PRESENTED AT CONFERENCES

Based on work performed under GA Technologies Inc. Internal Research and Development Funds.

1. Woolf, L.D., "Solar Photothermophotovoltaic Energy Conversion," poster presented at the 19th IEEE Photovoltaic Specialists Conference, 1987.

15. PATENT DISCLOSURES

Based on work performed under AFOSR Contracts F49620-86-C-0043 and F49620-84-C-0105.

1. Woolf, L.D., and J.C. Bass, "Direct Band Gap Solar Cell With Back Surface Reflector," to be submitted to U.S. Patent Office, 1987.

END

FEB.

1988

DTIC